communications biology

Article

https://doi.org/10.1038/s42003-024-06998-6

Deciphering the role of VapBC13 and VapBC26 toxin antitoxin systems in the pathophysiology of *Mycobacterium tuberculosis*

Arun Sharma[1], Neelam Singh[1,3], Munmun Bhasin[2,3], Prabhakar Tiwari[1], Pankaj Chopra[1], Raghavan Varadarajan[2] & Ramandeep Singh[1]

The expansion of VapBC TA systems in *M. tuberculosis* has been linked with its fitness and survival upon exposure to stress conditions. Here, we have functionally characterized VapBC13 and VapBC26 TA modules of *M. tuberculosis*. We report that overexpression of VapC13 and VapC26 toxins in *M. tuberculosis* results in growth inhibition and transcriptional reprogramming. We have also identified various regulatory proteins as hub nodes in the top response network of VapC13 and VapC26 overexpression strains. Further, analysis of RNA protection ratios revealed potential tRNA targets for VapC13 and VapC26. Using in vitro ribonuclease assays, we demonstrate that VapC13 and VapC26 degrade *serT* and *leuW* tRNA, respectively. However, no significant changes in rRNA cleavage profiles were observed upon overexpression of VapC13 and VapC26 in *M. tuberculosis*. In order to delineate the role of these TA systems in *M. tuberculosis* physiology, various mutant strains were constructed. We show that in comparison to the parental strain, Δ*vapBC13* and Δ*vapBC26* strains were mildly susceptible to oxidative stress. Surprisingly, the growth patterns of parental and mutant strains were comparable in aerosol-infected guinea pigs. These observations imply that significant functional redundancy exists for some TA systems from *M. tuberculosis*.

In the 1980s, a gene locus was identified in bacterial plasmids that promotes conjugative plasmid maintenance and kills host bacterial cells if they lose the plasmid[1–3]. These genetic modules were later named toxin-antitoxin (TA) systems. The toxin component of TA systems restricts bacterial growth by inhibiting essential cellular processes such as cell wall synthesis, cell division, DNA replication, transcription or protein synthesis[3–5]. In most cases, antitoxin binds tightly with the toxin and regulates its activity[4,6–9]. The advent of genome sequencing has resulted in the identification of a large number of TA systems that are encoded by either plasmids or bacterial chromosomes[7,10–12]. The primary physiological function of plasmid-encoded TA pairs is plasmid maintenance, whereas the function of chromosomal-encoded TA pairs is still being elucidated[1,6,13–15]. Numerous studies have implicated the importance of chromosomal encoded TA pairs in phage defence, stress response, antibiotic tolerance and bacterial virulence[13,14,16–20]. Despite the paucity of information regarding the physiological function of chromosomal TA pairs, significant advances have been achieved in understanding the mechanisms of growth inhibition by toxins and the neutralisation of toxin activity by their cognate antitoxins[21–30]. Based on the nature of antitoxin and its toxin-neutralizing mechanism, TA systems are classified into eight types (type I to type VIII)[7,31]. Antitoxins belonging to type I, III or VIII are RNA molecules that inactivate their cognate toxins by either binding to toxin transcript or protein. The antitoxins of the remaining types are proteinaceous in nature and inhibit the toxin activity by either directly binding to the toxin (type II, V, VI and VII) or by competing with the toxin for binding to its cellular targets (type IV)[7,31]. With the exception of the recently identified type VIII TA system, the majority of the toxins identified are proteinaceous in nature.

The genome of *M. tuberculosis* or MTBC complex encodes for a higher number of TA systems compared to non-pathogenic species[11,32]. These belong to either VapBC, MazEF, RelBE, HigBA, HicAB, DarTG, PezAT,

[1]Centre for Tuberculosis Research, Tuberculosis Research Laboratory, Translational Health Science and Technology Institute, Faridabad-Gurugram expressway, Faridabad, Haryana, India. [2]Molecular Biophysics Unit, Indian Institute of Science, Bangalore, Karnataka, India. [3]These authors contributed equally: Neelam Singh, Munmun Bhasin. e-mail: ramandeep@thsti.res.in

MbcTA, ParDE, and MenAT subfamily of TA systems[10,11,33–35]. Previous studies have demonstrated that most toxins impede bacterial growth when expressed ectopically, but this inhibition was reversed upon co-expression of their cognate antitoxin[11,32,36–38]. The VapBC subfamily of the type II TA system is most prevalent in *M. tuberculosis*; however, the pathophysiological significance for the majority of the members has not been thoroughly investigated. It has been shown that VapC toxins belonging to the VapBC family exhibit ribonuclease activity and are characterised by the presence of the PIN (piLT-N-terminus) domain[39]. The name refers to the amino-terminus domain of an annotated type IV pili twitching motility (PilT) protein[40]. The active site of VapC toxins comprises five to six acidic residues[41]. VapB antitoxins possess DNA-binding and toxin-binding domains at their amino- and carboxy-terminus, respectively[30,42]. The ectopic expression of VapC toxins suppresses *M. tuberculosis* growth by either cleaving the anticodon loop of tRNAs or the highly conserved Sarcin-Ricin loop (SRL) of 23S ribosomal RNA[18,22,25,43–46]. It has been shown that a subset of VapBC TA systems is differentially expressed following exposure to stress conditions, and these might contribute to *M. tuberculosis* survival in these conditions in a cumulative manner[32,37,47]. Recently, it has been shown that the simultaneous deletion of eight TA systems in *M. smegmatis* resulted in decreased mycobacteriophage infection and survival during nutrient-limiting conditions[48]. We have previously shown that deletion of either VapBC3, VapBC4, VapBC11 or VapC22 impairs the ability of *M. tuberculosis* to establish disease in guinea pigs[17,25,37]. We have also reported that MazF3, MazF6 and MazF9, HigB1, MenT2 or MenT3 and MenT4 also contribute to the pathogenesis of *M. tuberculosis* in guinea pigs[38,49–51]. However, the intracellular growth of parental or *M. tuberculosis* strains with deletions in either *vapC21*, *vapC28* or *darTG* were comparable in vivo[37,52,53]. In addition to stress adaptation and pathogenesis, it has been demonstrated that ectopic expression of free toxins such as VapC21, RelE1, RelE2 or MazF3 contributes to the formation of drug-tolerant bacteria[49,54,55].

Based on sequence and structure similarity, VapBC TA systems from *M. tuberculosis* have been categorised into distinct clusters[11]. In the present study, we have functionally characterized VapBC13 and VapBC26 TA systems of *M. tuberculosis*. We show that overexpression of either VapC13 or VapC26 resulted in reduced in vitro growth of *M. tuberculosis*. RNA-Seq analysis revealed that ectopic expression of VapC13 and VapC26 led to the upregulation of transcripts that encode for proteins necessary for *M. tuberculosis* survival upon exposure to oxidative stress. We also observed a decline in protection ratios in the cleavage profile of a subset of tRNAs upon overexpression of either VapC13 or VapC26. The rRNA cleavage profiles obtained from parental, VapC13 and VapC26 overexpression strains were similar. We also demonstrate that *serT* and *leuW* are in vitro degraded by VapC13 and VapC26, respectively. Furthermore, we show that deletion of either VapBC13 or VapBC26 from the *M. tuberculosis* genome mildly increased its susceptibility towards oxidative stress. However, both VapC13 and VapC26, alone or in complex with VapB13 and VapB26, respectively, were dispensable for *M. tuberculosis* growth in guinea pigs. Taken together, we have performed a detailed study to decipher the role of VapBC13 and VapBC26 TA pairs in *M. tuberculosis* physiology and pathogenesis.

Results

VapC13 overexpression inhibits the growth and significantly alters the transcriptome of *M. tuberculosis*

Previously, it has been demonstrated that overexpressing a subset of VapC toxins using an IPTG, acetamide or Atc inducible vector inhibits the growth of *E. coli, M. smegmatis, M. bovis* BCG or *M. tuberculosis*[10,22,32,37,56]. As reported earlier, we show that inducible expression of the VapC13 toxin inhibited *M smegmatis* and *M. tuberculosis* growth (Supplementary Fig. S1A and Fig. 1A)[37]. Immunoblot analysis confirmed the expression of myc-tagged VapC13 in the cytosolic fraction of recombinant *M. smegmatis* strain (Supplementary Fig. S1B). We have previously reported that transcription profiles of *M. tuberculosis* are significantly altered upon overexpression of toxins such as VapC11, VapC21, VapC22 or MazF6[17,25,37,57]. We hypothesize that the expression of these toxins leads to reduced metabolism, and this transcription reprogramming enables the bacteria to adapt to stress conditions[17,25,49,57]. In the present study, we investigated the effect of VapC13 overexpression on the transcription profiles of *M. tuberculosis*. We performed differential gene expression analysis on the reads acquired from three biological replicates. The differentially expressed genes (DEGs) were filtered using a cut-off *P value* of <0.05 and fold change of either >2.0 or < −2.0. Using this cut-off, we observed that compared to the strain harbouring the vector control, a total of 1326 genes were differentially expressed in the *M. tuberculosis* strain overexpressing VapC13 (Supplementary Data Set 1). The expression of 605 and 721 transcripts was increased and decreased, respectively, in the VapC13 overexpression strain relative to the parental strain (Fig. 1B, Supplementary Data Set 1). The annotation of DEGs according to functional categories revealed that the majority of transcripts with increased levels encoded for either conserved hypothetical proteins or proteins involved in intermediary metabolism and respiration or cell wall processes (Table 1). The expression profiles of 34, 33 and 22 transcripts obtained upon overexpression of VapC13 in *M. tuberculosis* were similar to those obtained upon exposure to enduric hypoxia response (EHR) or nutrient starvation or oxidative stress, respectively[58–60] (Supplementary Fig. S2A–C). In order to gain insights into the biological processes that were differentially regulated upon overexpression of VapC13 in *M. tuberculosis*, the NCBI-based tool DAVID (Database for Annotation Visualization and Integrated Discovery) was used[61]. In the VapC13 overexpression strain, we observed increased levels of transcripts encoding for proteins involved in biological processes such as translation, growth regulation, DNA repair and response to copper and antibiotics (Supplementary Fig. S3A). The majority of the transcript with increased expression in the biological process of translation encoded for ribosomal proteins (Supplementary Data Set 1). We also noticed that in comparison to the strain harbouring vector control, transcript levels of various regulatory proteins such as Rv2034, Rv2642, Rv3066, Rv3334, WhiB5, WhiB6 and EmbR were increased in *M. tuberculosis* upon overexpression of VapC13 (Supplementary Data Set 1). The levels of transcripts encoding for proteins implicated in the bacterial response to metal ions such as MymT, CsoR, Rv0968, CtpV, LpqS and Rv0190 were significantly increased in the VapC13 overexpression strain relative to the control strain (Supplementary Data Set 1)[62–64]. As shown in Table 1, we observed that in the VapC13 overexpression strain of *M. tuberculosis*, ~32% of the transcripts with reduced expression encoded for proteins involved in intermediary metabolism and respiration. In agreement, DAVID analysis of DEGs with reduced expression revealed that expression of genes encoding for proteins involved in biological processes such as respiration, ATP synthesis and tricarboxylic cycle were significantly affected in the VapC13 overexpression strain (Supplementary Fig. S3B). The transcript levels of genes encoding for proteins involved in lipid metabolism, such as *pks2*, *pks3*, *pks4*, *mmpl10*, *papA1*, and, *papA3* were also significantly decreased in the VapC13 overexpression strain as compared to the strain harbouring the vector control (supplementary data set 1). Previously, it has been shown that these proteins are involved in the synthesis and transport of virulence-associated lipids such as 2,3-di-O-acyl-trehalose, poly-acyl trehalose and sulfolipids[65,66]. In addition to these, the levels of transcripts encoding for proteins involved in host-pathogen interactions such as LprK, Mce1A, Mce1B, Mce1C, Mce1D, Mce1F, FadD13, FadE28, FadA2, SugB and SugC were also reduced in the VapC13 overexpression strain (Supplementary Data Set 1)[67–69]. In conclusion, our data suggest that the ectopic expression of VapC13 results in growth inhibition and alteration of transcriptional profiles in *M. tuberculosis*. This transcriptional reprogramming might be associated with reduced metabolism, altered lipid biosynthesis and adaptation of *M. tuberculosis* in host tissues.

Differential gene expression analysis upon overexpression of VapC26 in *M. tuberculosis*

Previous studies have identified that most VapC homologues from *M. tuberculosis* cleave the anticodon loop of tRNA except for VapC20 and VapC26[18,22,43–46]. VapC20 and VapC26 are phylogenetically related and known to cleave the highly conserved SRL of 23S ribosomal RNA[22,43].

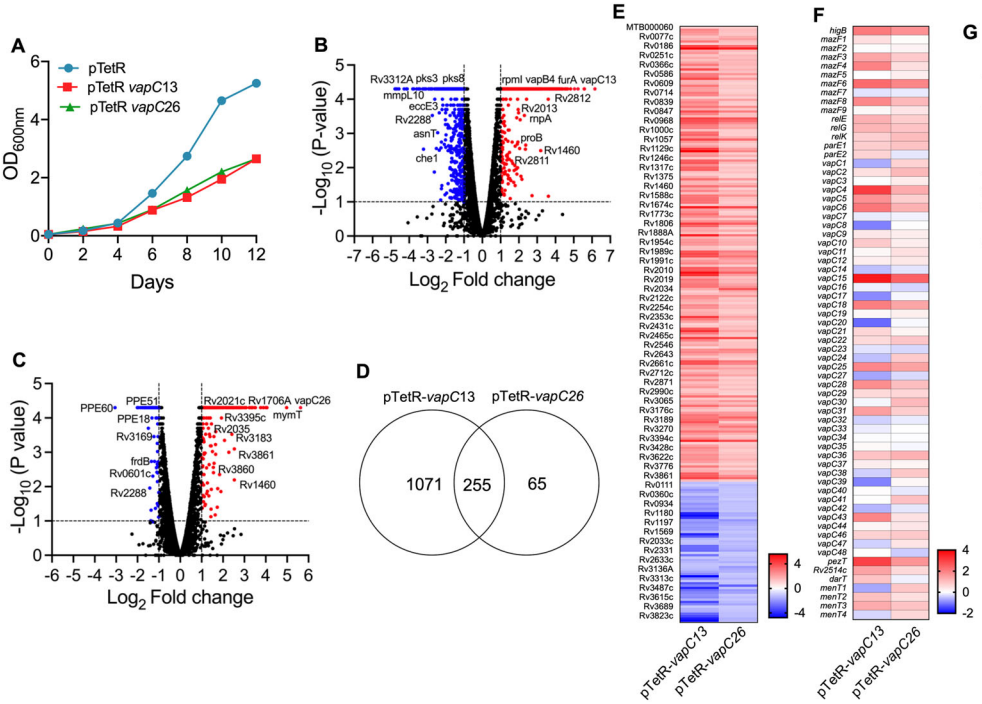

Fig. 1 | Effect of VapC13 and VapC26 overexpression on the growth and transcriptional profiles of *M. tuberculosis*. **A** The overexpression of either VapC13 or VapC26 using anhydrotetracycline inducible vector inhibits *M. tuberculosis* growth. The data shown in this panel is representative of two independent experiments. The overexpression of VapC13 (**B**) and VapC26 (**C**) in *M. tuberculosis* resulted in the differential expression of 1326 and 320 genes, respectively. Volcano plots represent the genes with increased (red dots), decreased (blue dots) or unchanged expression (black dots) in VapC13 and VapC26 overexpression strains in comparison to the strain harbouring the vector control. **D** Venn diagram showing comparative analysis of differentially expressed genes obtained in VapC13 and VapC26 overexpression strains of *M. tuberculosis*. **E** Heat maps showing fold changes of the differentially expressed genes common in VapC13 and VapC26 overexpression strains of *M. tuberculosis*. **F** Heatmaps depicting fold change in the relative transcript levels of non-cognate toxins in VapC13 and VapC26 overexpression strains of *M. tuberculosis*. The colour intensity in heatmaps (**E** and **F**) represent the $\log_2$ value of the fold change. The data shown in panels **B**–**F** is obtained from three biological replicates. Quantitative real-time PCR was performed to determine the expression levels of a subset of DEGs in VapC13 (**G**) and VapC26 (**H**) overexpression strains. The data obtained was normalized to the levels of *sigA* and is shown as mean + SD of $\log_2$ of fold change obtained from three independent experiments. Source data is provided in Supplementary Data Set 4.

In agreement with previous studies, we show that overexpression of VapC26 inhibited both *M. smegmatis* and *M. tuberculosis* growth[22,37] (Fig. 1A and Supplementary Fig. S1C). As shown in Supplementary Fig. S1D, we observed the expression of myc-tagged VapC26 in the cytosolic fraction of the recombinant *M. smegmatis* strain. In the present study, we also performed experiments to determine the transcriptional changes upon overexpression of an SRL-cleaving toxin, VapC26, in *M. tuberculosis*. Using a cut-off value of fold change of >2.0 or <−2.0 and a *P-value* < 0.05, we observed that the expression of 320 transcripts was significantly altered upon overexpression of VapC26 in *M. tuberculosis* (Fig. 1C, Supplementary Data Set 2). Amongst these, the levels of 226 and 94 transcripts were increased and decreased, respectively, in the VapC26 overexpression strain relative to the strain harbouring the vector control (Fig. 1C). The majority of the transcripts with increased expression encoded for either conserved hypothetical proteins or regulatory proteins or proteins involved in virulence of *M. tuberculosis* (Table 1). In the VapC26 overexpression strain, the transcript levels of several regulatory proteins such as WhiB1, WhiB6, WhiB7, Rv2034, CmtR, Rv0474, Rv0195, PknH and EthR were increased in comparison to the strain harbouring the vector control (Supplementary Data Set 2). As observed in the case of the VapC13 overexpression strain, a subset of transcripts differentially expressed in the VapC26 overexpression strain were also differentially expressed in *M. tuberculosis* after exposure to various stress conditions such as low oxygen, nutritional and oxidative stress (Supplementary Fig. S2D–F). DAVID analysis of the upregulated DEGs revealed that genes involved in biological processes such as transcription regulation, response to copper, cadmium ions, host immune response and growth regulation were significantly enriched in the VapC26 overexpression strain (Supplementary Fig. S3C). In our RNA-Seq data, we noticed that the levels of transcripts such as *ahpC*, *hsp* and *furA* involved in bacterial adaptation to oxidative stress and redox homoeostasis were significantly increased upon VapC26 overexpression (Supplementary Data Set 2). The transcripts encoding for various redox regulators such as *sigE*, *lsr2*, *whiB1*, and *whiB6* were also increased in *M. tuberculosis* upon VapC26 overexpression[70,71] (Supplementary Data Set 2). According to mycobrowser and DAVID-based annotation, we noticed that the majority of transcripts with decreased expression in the VapC26 overexpression strain encoded for proteins involved in the cell wall and related metabolic processes (Table 1, Supplementary Fig. S3D). These included secretory proteins such as SapM, Mpt53 and cell-envelope associated proteins such as Apa, EspC, EspA and LpqG (Supplementary Data Set 2)[72–77]. As shown in Supplementary Data Set 2, the top five transcripts with reduced expression in the VapC26 overexpression strain encode for the PE/PPE_PGRS family of proteins. Previously, it has been shown that the PE/PPE_PGRS family of proteins contributes to host-pathogen interactions and virulence of *M. tuberculosis*[78]. Taken together, this data indicates that the presence of free VapC26 might be associated with significant changes in *M. tuberculosis* cell wall and oxidative stress responses, which are important for the intracellular survival of *M. tuberculosis*.

The transcription profiles obtained upon overexpression of VapC13 and VapC26 revealed significant similarities

We observed that the expression patterns of 255 transcripts were similar in *M. tuberculosis* strains overexpressing either VapC13 or VapC26 (Fig. 1D). In both VapC13 and VapC26 overexpression strains, the levels of transcripts

Table 1 | Mycobrowser-based annotation of differential expressed genes obtained in VapC13 and VapC26 overexpression strains relative to the strain harbouring the vector control

S. no.	Functional Category	No. of DEGs with increased expression (VapC13^{OE})	No. of DEGs with reduced expression (VapC13^{OE})	No. of DEGs with increased expression (VapC26^{OE})	No. of DEGs with reduced expression (VapC26^{OE})
1.	Cell wall and cell processes	87	151	25	27
2.	Conserved hypotheticals	193	156	73	22
3.	Information pathways	65	23	12	3
4.	Insertion seqs and phages	27	7	8	2
5.	Intermediary metabolism and respiration	89	233	23	18
6.	Lipid metabolism	18	83	5	9
7.	PE/PPE	31	10	13	8
8.	Regulatory proteins	45	13	33	1
9.	Stable RNAs	4	6	1	0
10.	Unknown	3	1	1	0
11.	Virulence, detoxification, adaptation	43	38	32	4

The data was obtained from 3 biological replicates.

such as *whiB1*, *sigE*, *whiB7*, *ahpC*, *trxB1* and *hsp* that encode for proteins involved in redox homoeostasis and adaptation of *M. tuberculosis* to oxidative stress were increased relative to the strain harbouring the vector control (Fig. 1E, Supplementary Data Set 1 and Supplementary Data Set 2). Previously, it has been shown that TA systems are also regulated in a post-transcriptional manner. In *E. coli*, it has been reported that the *relBEF* operon is activated by the ectopic expression of non-cognate toxins such as MazF, MqsR, HicA and HipA toxins[79]. Also, the activation of *mazEF* during amino acid starvation depends on the *relBE* TA system[79]. Similar to *E. coli*, transcriptional cross-activation has also been reported among TA systems in *M. tuberculosis*[37]. In our RNA-Seq experiment, we also observed the regulatory interplay between type II TA systems. We noticed that the transcripts encoding for non-cognate toxins such as *vapC25*, τ toxin (Rv0366c), *vapC4*, *vapC28*, *vapC6*, *mazF6*, *vapC15*, *mazF8* and *vapC18* were significantly increased in *M. tuberculosis* strains overexpressing either VapC13 or VapC26 (Fig. 1F, Supplementary Data Set 1 and Supplementary Data Set 2). Further, the inducible overexpression of VapC13 in *M. tuberculosis* also resulted in increased levels of transcripts encoding for other non-cognate toxins such as *higB1*, Rv2514c, *vapC5*, *vapC31*, *vapC43*, *mazF3*, *mazF4*, *relE* and *relG* toxins (Fig. 1F, Supplementary Data Set 1). The overexpression of VapC26 resulted in increased levels of transcripts encoding for other non-cognate toxins such as *vapC2*, *vapC30* and *vapC36* in *M. tuberculosis* (Fig. 1F and Supplementary Data Set 2). These observations suggest that ectopic expression of either VapC13 or VapC26 results in the activation of canonical and non-canonical TA pairs in *M. tuberculosis*. We also noticed that DEGs common in VapC13 or VapC26 overexpression strains exhibited similar expression patterns. The differential expression of a subset of these DEGs in VapC13 and VapC26 overexpression *M. tuberculosis* strains relative to the parental strain was confirmed by qPCR (Fig. 1G, H). Taken together, we observed that in comparison to the strain harbouring the vector control, expression of genes encoding for proteins involved in adaptation to oxidative stress, redox homoeostasis or non-cognate toxins were increased in *M. tuberculosis* upon overexpression of either VapC13 or VapC26.

Network Analysis and tRNA substrate predictions for VapC13 and VapC26

We also performed a detailed network analysis to further investigate the transcriptional profiles obtained from the parental and VapC13 or VapC26 overexpression strain. There are 3686 proteins (nodes) and 34,223 molecular interactions (edges) in the protein-protein interaction network *of M. tuberculosis*[80]. In the case of the VapC13 overexpression strain, the top-ranked paths generated a subnetwork with 289 nodes (Supplementary Fig. S4). Amongst these, 123 were DEGs that had significant changes in gene expression in the VapC13 overexpression strain relative to the strain harbouring the vector control (Supplementary Data Set 1). In comparison, overexpression of VapC26 in *M. tuberculosis* resulted in a subnetwork with 326 nodes comprising 51 DEGs (Supplementary Fig. S5). The subnetworks were further examined to identify hub nodes (nodes with a high number of interactions with other nodes) and to analyse the overlap between them. In our network analysis, Rv2034 was identified as a common hub node in VapC13 and VapC26 overexpression strains (Fig. 2A, Supplementary Figs. S4 and S5). In our RNA-Seq data analysis, the transcript levels for Rv2034 were increased by ~4.0-fold and 13.5-fold in *M. tuberculosis* strains overexpressing VapC13 and VapC26, respectively (Supplementary Data Set 1 and 2). Rv2034 belongs to the ArsR family of transcriptional regulators and is a positive regulator of PhoP and DosR response regulators with a possible role in lipid metabolism and adaptation to low oxygen growth conditions[81]. In addition, other regulatory proteins such as Rv2011c and Rv1990c were also identified as hub nodes in VapC13 and VapC26 overexpression strain network analysis (Fig. 2B, C, Supplementary Figs. S4 and S5). According to the Pfam database, Rv2011c belong to the MarR family of transcriptional regulators[82,83]. Rv1990c has been characterized as an antitoxin that harbours an XRE-like HTH domain[34]. We also identified Rv1129c, Rv1044 and Rv2307B as hub nodes in network analysis obtained from the VapC13 overexpression strains (Supplementary Fig. S4). The expression of Rv1129c, Rv1044 and Rv2307B was increased by ~20.0, 5.0 and 4.0-fold, respectively, in VapC13 overexpression strain relative to the vector only control (Supplementary Data Set 1). In networks obtained from the VapC26 overexpression strain, Rv2022c was identified as an additional hub node (Supplementary Fig. S5). The expression of Rv2022c was increased by ~5.0-fold in VapC26 overexpression strain (Supplementary Data Set 2). Surprisingly, no hub nodes were identified with reduced expression in *M. tuberculosis* upon overexpression of either VapC13 or VapC26. These findings imply that overexpressing either VapC13 or VapC26 alters the transcriptional profiles of *M. tuberculosis*.

Previous studies have shown that VapC toxins possess endoribonuclease activity and inhibit protein translation by mostly cleaving either tRNA or rRNA[18,22,44–46]. The cellular target for VapC13 is still unknown, but it has been shown that VapC26 cleaves the SRL of 23S rRNA[22]. We, therefore, analysed RNA-Seq data obtained from VapC13 and VapC26 overexpression strains of *M. tuberculosis* to identify their plausible tRNA or rRNA targets. The cleavage specificities for each tRNA and rRNA were evaluated by examining the cleavage profiles across the transcriptome and

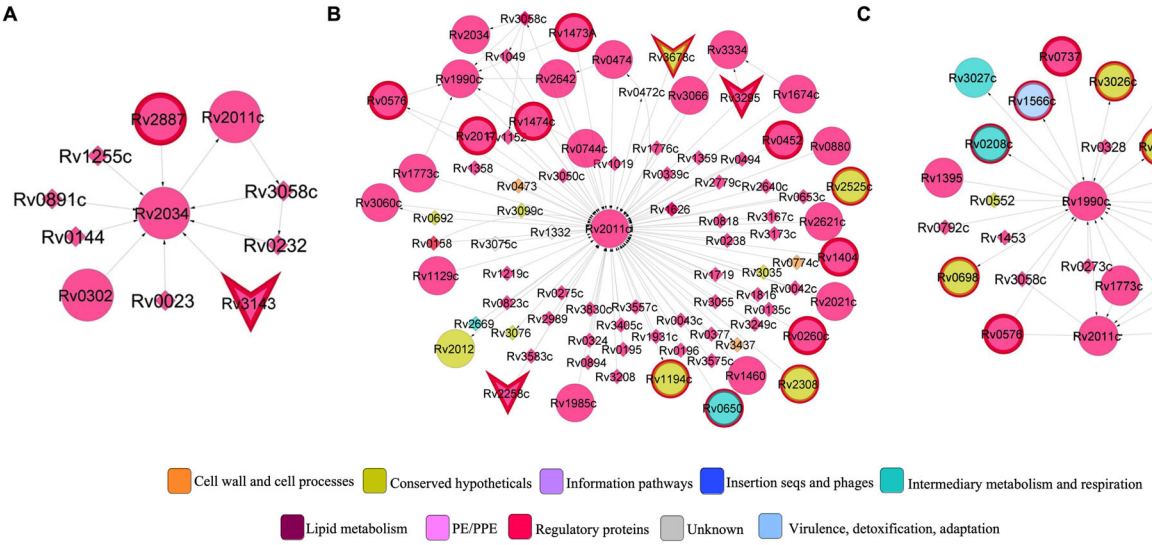

Fig. 2 | Network analysis of differentially regulated transcripts from overexpression of VapC13 or VapC26 in *M. tuberculosis*. The RNA-Seq data of parental, VapC13 and VapC26 overexpression strains was compared in a network depicting the top responses of nodes or genes. The network of differentially expressed common hub nodes, Rv2034 (**A**), Rv2011c (**B**) and Rv1990c (**C**), upon overexpression of VapC13 and VapC26 in *M. tuberculosis* are presented. These nodes are coloured according to their functional categories in mycobrowser. The shape of the nodes reflects the gene expression pattern. The circles and arrowheads represent the nodes with increased or decreased expression, respectively. The diamonds represent the genes that showed comparable expression levels in vector and toxin overexpression strains.

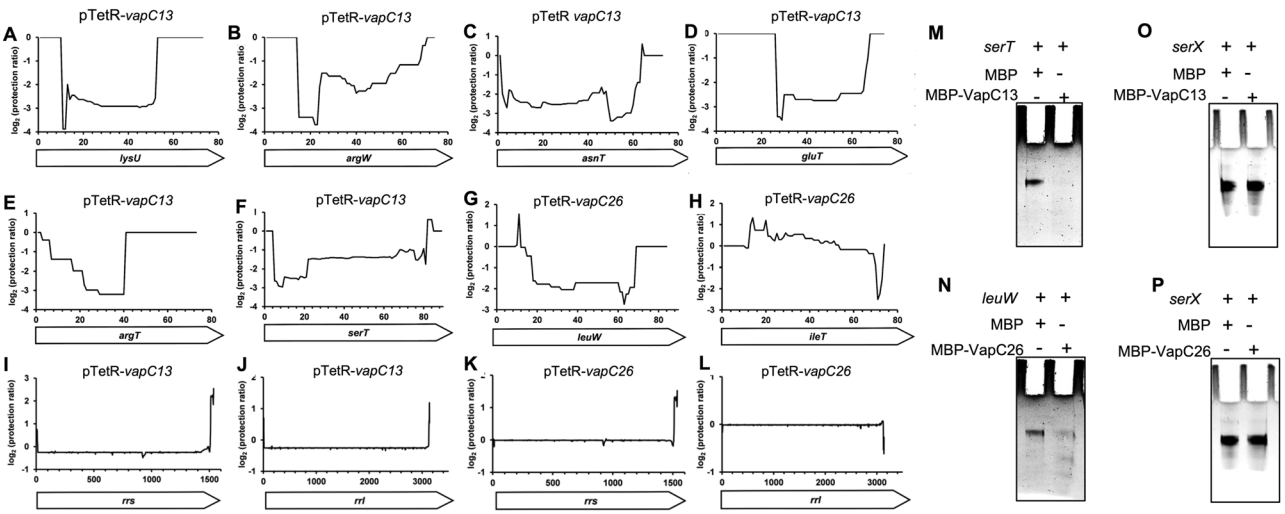

Fig. 3 | Effect of VapC13 and VapC26 overexpression on the tRNA cleavage profile of *M. tuberculosis*. **A**–**L** The $\log_2$ (protection ratio) for various tRNAs in VapC13 (**A**–**F**) and VapC26 (**G**, **H**) overexpression strain relative to the parental strain is shown in this panel. The profiles for 16S and 23S rRNA obtained in VapC13 (**I**, **J**) and VapC26 (**K**, **L**) overexpression strains are shown in comparison to the parental strain. The x-axis represents the nucleotide position of the respective tRNA (**A**–**H**) and rRNA (**I**–**L**). The data shown in panels **A**–**L** is obtained from three biological replicates. In vitro *serT* (**M**), *leuW* (**N**) and *serX* (**O** and **P**) cleavage assays were performed with various purified proteins as described in materials and methods. The in vitro cleavage reactions were resolved on 15% UREA-PAGE and visualized by EtBr staining. The data shown in panels **M**–**P** is representative of two independent experiments. Source data is provided in Supplementary Data Set 4.

calculating the $\log_2$ protection ratios at each nucleotide position, as described in Materials and Methods[57]. In our data analysis, a stringent threshold of $\log_2$ (protection ratio) ≤ −2.5 was considered to predict tRNA or rRNA cellular targets for VapC13 and VapC26. We observed lower protection ratios for the transcripts of several tRNAs such as *lysU* (tRNA-Lys^{CTT}), *argW* (tRNA-Arg^{TCT}), *asnT* (tRNA-Asn^{GTT}), *gluT* (tRNA-Glu^{TTC}), *argT* (tRNA-Arg^{CCT}) and *serT* (tRNA-Ser^{GCT}) in *M. tuberculosis* overexpressing VapC13 relative to the parental strain (Fig. 3A–F, Supplementary Data Set 3). In the case of VapC26 overexpression strains, transcripts for *leuW* (tRNA-Leu^{TAG}) and *ileT* (tRNA-Ile^{GAT}) showed low protection ratios relative to the strain harbouring the vector control (Fig. 3G, H, Supplementary Data Set 3). The protection ratios for remaining tRNAs were comparable in parental, VapC13 and VapC26 overexpression strains (Supplementary Data Set 3). Next, we performed in vitro ribonuclease cleavage assays using purified proteins and *serT* or *leuW* as representative targets for VapC13 and VapC26, respectively. In agreement with the RNA-Seq based cleavage profiles, we show that purified MBP-VapC13 and MBP-VapC26 degrade *serT* and *leuW*, respectively (Fig. 3M, N). These observations are in agreement with the observed cleavage profiles, where, we observed a significant decrease in the protection ratio for a large part of these transcripts. As expected, no degradation of *serT* and *leuW* was observed in the presence of purified MBP protein (Fig. 3M, N). Also, purified

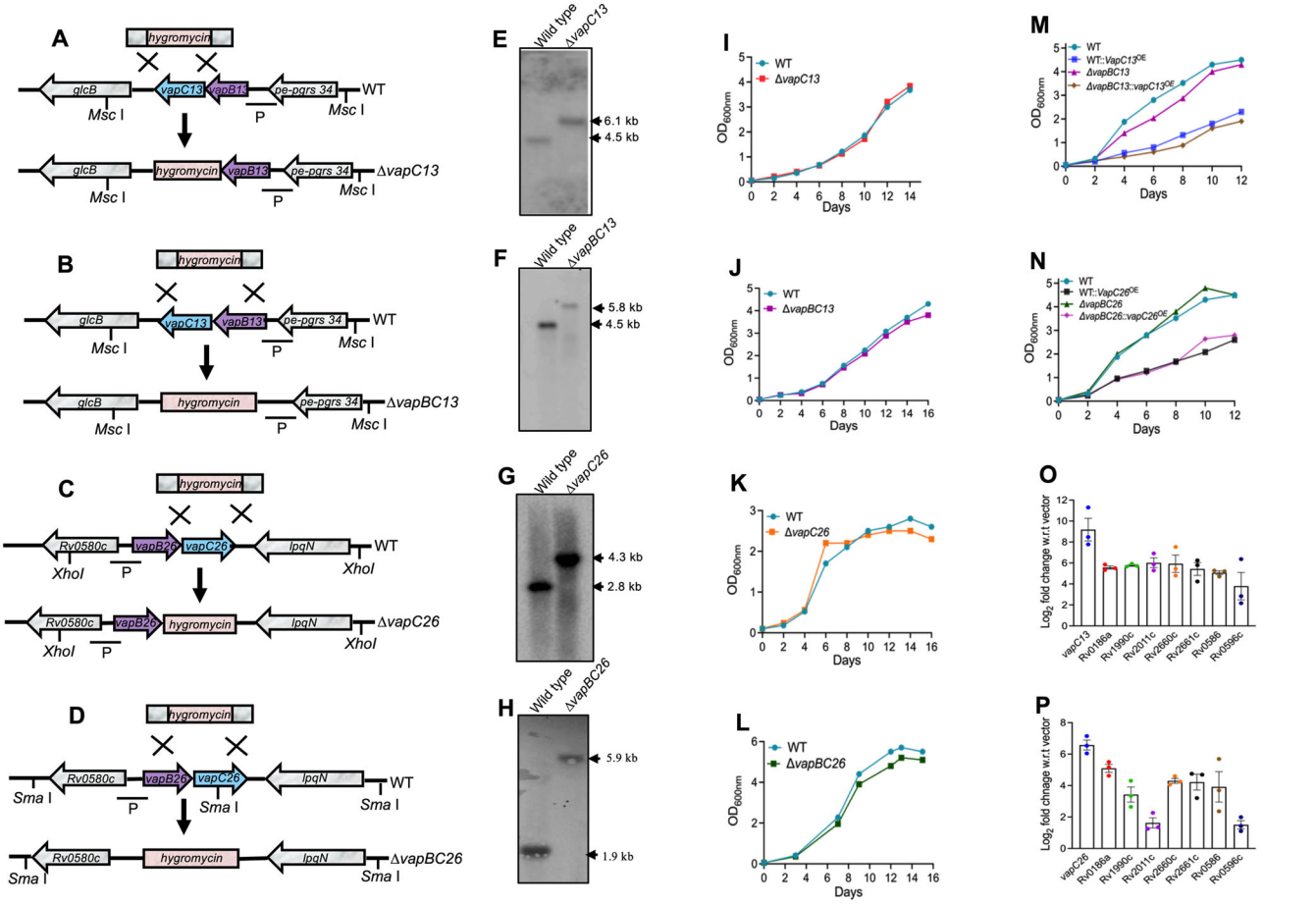

Fig. 4 | VapBC13 and VapBC26 TA systems are dispensable for the in vitro growth of *M. tuberculosis*. Schematic representation of *vapC13* (**A**), *vapBC13* (**B**), *vapC26* (**C**) and *vapBC26* (**D**) TA loci in wild type and respective mutant strains. The construction of Δ*vapC13* (**E**), Δ*vapBC13* (**F**), Δ*vapC26* (**G**) and Δ*vapBC26* (**H**) was confirmed by Southern blot. **I**–**L** The growth pattern of parental and various mutant strains was compared by measuring OD_{600nm} at regular intervals. The over-expression of VapC13 (**M**) or VapC26 (**N**) using an anhydrotetracycline inducible vector inhibits the growth of Δ*vapBC13* and Δ*vapBC26* strain, respectively. The data shown in panels **I**–**N** is representative of two independent experiments. Quantitative real-time PCR was performed to determine the expression levels of a subset of DEGs obtained upon VapC13 (**O**) or VapC26 (**P**) overexpression in the Δ*vapBC13* or Δ*vapBC26* mutant background, respectively. The data obtained was normalized to *sigA* levels and is shown as mean ± SD of $\log_2$ of fold change obtained from three independent experiments. Source data is provided in Supplementary Data Set 4.

MBP-VapC13 and MBP-VapC26 proteins were unable to degrade the non-specific control tRNA molecule, *serX*, confirming the absence of non-specific ribonuclease contamination in the protein preparation (Fig. 3O, P). We also compared the rRNA profiles obtained from vector only, VapC13 and VapC26 overexpression strains. Intriguingly, we did not observe any differences in 23S and 16S rRNA cleavage profiles obtained from VapC26 overexpression strains relative to the parent strain despite 16.0-fold increased transcript levels of *vapC26* in the overexpression strain (Figs. 1H and 3K, L). We did not observe any significant changes in the cleavage profiles of 16S and 23S rRNA in the VapC13 overexpression strain relative to the parental strain (Fig. 3I, J). Taken together, analysis of cleavage profiles of tRNA and rRNAs across the transcriptomes of VapC13 and VapC26 overexpression strain provides insights into the putative cellular targets of these toxins in their native host *M. tuberculosis*.

Deletion of VapBC13 and VapBC26 genes does not alter the in vitro growth characteristics of *M. tuberculosis*

In the present study, we further performed experiments to understand the role of the VapBC13 and VapBC26 TA systems in the physiology and pathogenesis of *M. tuberculosis*. *M. tuberculosis* strains with deletions in either *vapC13, vapBC13, vapC26* or *vapBC26* were constructed using temperature-sensitive mycobacteriophages (Fig. 4A–D). The replacement of *vapC13* and *vapBC*13 with the hygromycin resistance gene was confirmed by Southern blot. As shown in Fig. 4E, F, the locus-specific probe hybridized with 6.1 and 5.8 kb region in *Msc* I digested genomic DNA from Δ*vapC13* and Δ*vapBC13* mutant strains of *M. tuberculosis*, respectively. As expected, the probe hybridized to a 4.5 kb region in *Msc* I digested genomic DNA from the wildtype strain (Fig. 4E, F). The replacement of *vapC26* with the hygromycin resistance gene was confirmed by Southern blot. The locus-specific probe hybridized with 2.8 kb and 4.3 kb region in *Xho* I digested genomic DNA isolated from wild type and Δ*vapC26 M. tuberculosis* strain, respectively (Fig. 4G). To verify the construction of Δ*vapBC26* strain, genomic DNA was isolated from wildtype and Δ*vapBC26* strain and digested with *Sma* I. As shown in Fig. 4H, the probe hybridized with a 1.9 kb fragment in the lane corresponding to wild type strain. The replacement of *vapBC26* with a hygromycin resistance cassette resulted in the loss of *vapC26* internal *Sma* I restriction site (Fig. 4D). Therefore, the locus-specific probe hybridized to a 5.9 kb fragment in the lane corresponding to Δ*vapBC26* strain (Fig. 4H). Earlier studies suggest that deletion of toxin alone (*vapC21* or *higB1* or *menT2* or *vapC28*) or toxin and antitoxin (*vapBC3 or vapBC4 or vapBC11 or darTG*) is dispensable for *M. tuberculosis* growth in vitro[25,37,38,49,53]. We observed that deleting either *vapC13*, *vapBC13*, *vapC26*, or *vapBC26* did not alter the in vitro growth of *M. tuberculosis* in 7H9 medium till the stationary phase was attained (Fig. 4I–L). In agreement with our earlier observations, we observed that inducible expression of either VapC13 or VapC26 also inhibited the growth of Δ*vapBC13* and Δ*vapBC26*,

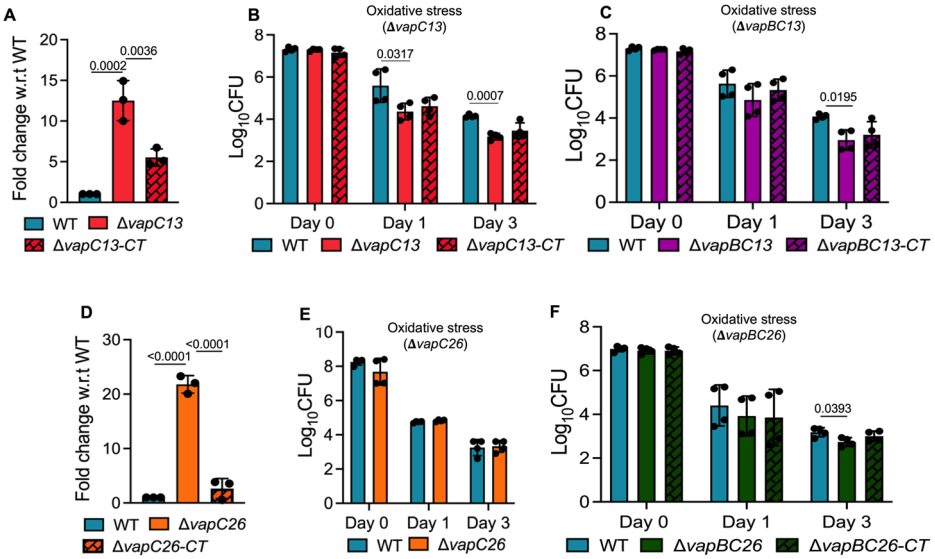

Fig. 5 | VapBC13 and VapBC26 are required for the survival of *M. tuberculosis* during oxidative stress conditions. The transcript levels of *vapB13* (**A**) and *vapB26* (**D**) were measured in Δ*vapC13* and Δ*vapC26* strains, respectively, by quantitative real-time PCR using gene-specific primers. The data obtained was normalized to *sigA* and is shown as the mean ± SD of fold change obtained from three independent experiments. **B**, **C**, **E**, **F** The bacterial loads of various strains were determined after exposure to 5 mM H_2O_2 for either 24 h or 72 h. The data shown in these panels is the mean ± SD of data obtained from two independent experiments performed in duplicates. *P values* depicted on the graphs were assessed using one-way ANOVA. Source data is provided in Supplementary Data Set 4.

respectively (Fig. 4M, N). The observed growth inhibition pattern was similar to that obtained from the overexpression of VapC13 and VapC26 in the parental strain of *M. tuberculosis*. Further, we also observed increased expression of a subset of DEGs validated in Fig. 1G, H upon overexpression of VapC13 and VapC26 in Δ*vapBC13* and Δ*vapBC26*, respectively (Fig. 4O, P). TA systems such as YafQ/DinJ, MazEF and MqsRA have been shown to be important for biofilm formation in *E. coli*[16,84]. Next, we compared the ability of parental and various mutant strains to form biofilms in detergent-free Sauton's medium. We observed that the ability of parental, Δ*vapC13*, Δ*vapBC13*, Δ*vapC26* and Δ*vapBC26* mutant strains to form biofilms was comparable (Supplementary Fig. S6A–D). Together, these findings imply that deletion of either *vapC13*, *vapBC13*, *vapC26*, or *vapBC26* did not affect *M. tuberculosis*'s ability to grow in vitro or form biofilms.

VapBC13 and VapBC26 TA systems are required for *M. tuberculosis* survival upon exposure to oxidative stress in vitro

The antitoxins belonging to the type II systems harbour a DNA binding motif at the amino terminus and bind to their native promoter with low affinity[85,86]. The C-terminal domain of antitoxin binds to their cognate toxin, and the TA complex subsequently binds to the native promoter with enhanced affinity[85,86]. This conditional co-operativity results in auto-repression from the native promoter[87,88]. Hence, we hypothesized that deleting either *vapC13* or *vapC26* from the genome of *M. tuberculosis* might result in derepression and increased transcript levels of *vapB13* and *vapB26* in Δ*vapC13* and Δ*vapC26*, respectively. In agreement, we noticed that relative to the parental strain, the transcript levels of *vapB13* and *vapB26* were increased by ~12.5-fold and ~20.0-fold in Δ*vapC13* and Δ*vapC26* strains, respectively (Fig. 5A, D). As shown in Fig. 5A, D, the levels of antitoxins were partially restored in the Δ*vapC13* complemented, and Δ*vapC26* complemented strains. *M. tuberculosis* is a highly successful intracellular pathogen as it is able to withstand diverse stress conditions during infection by reprogramming its transcription and growth[89,90]. It has been hypothesized that since a subset of TA systems are differentially expressed in *M. tuberculosis* upon exposure to stress conditions and these might contribute cumulatively to the adaptation of *M. tuberculosis* under these growth conditions[32,37,47]. We have previously reported that compared to parental strain, *M. tuberculosis* strains with deletions in either *mazF3*, *mazF6* and *mazF9* or *vapBC11* or *vapC22* or *menT3* and *menT4* were more susceptible to oxidative stress[17,25,38,51]. However, deleting either *vapBC3, vapBC4, vapC28, vapC21 or higB1* toxins had no phenotypic effect on *M. tuberculosis* growth under in vitro stress conditions[37,49,50,53]. Next, we compared the survival of wild type, Δ*vapC13*, Δ*vapBC13*, Δ*vapC26*, and Δ*vapBC26* upon exposure to in vitro stress conditions that *M. tuberculosis* encounters inside host tissues[91]. We show that compared to the parental strain, the Δ*vapC13* mutant strain displayed ~17.0-fold and 9.5-fold higher susceptibility after exposure to oxidative stress for 24 h and 72 h, respectively (Fig. 5B). This growth defect associated with the Δ*vapC13* mutant strain was partially restored by ~ 2.0-fold in the Δ*vapC13* complemented strain after exposure to oxidative stress for 24 h or 72 h (Fig. 5B). As shown in Fig. 5E, the survival of both parental and Δ*vapC26* mutant strains was comparable after exposure to oxidative stress. We have previously shown that the increased expression of VapB22 antitoxin in the Δ*vapC22* mutant strain might be responsible for the growth defect associated with the mutant strain upon exposure to oxidative stress and in host tissues[17]. We hypothesized that the increased susceptibility of the Δ*vapC13* mutant strain upon exposure to oxidative stress might be associated with either the deletion of *vapC13* or increased expression of cognate antitoxin, *vapB13*. In order to further delineate the role of VapBC13 in *M. tuberculosis* physiology, we compared the susceptibility of parental and Δ*vapBC13* strains after exposure to oxidative stress for either 24 h or 72 h. In agreement with the data obtained for the Δ*vapC13* mutant strain, we show that deletion of both *vapB13* and *vapC13* increased the susceptibility of *M. tuberculosis* towards oxidative stress (Fig. 5C). As shown in Fig. 5C, relative to the parental strain, survival of the Δ*vapBC13* mutant strain was reduced by ~ 13.0-fold after exposure to oxidative stress for 72 h. The mutant strain showed a growth defect of ~6.0-fold relative to the parental strain at 24 h post-exposure to oxidative stress (Fig. 5C). Interestingly, we also noticed that deletion of *vapBC26* increased the susceptibility of *M. tuberculosis* to oxidative stress (Fig. 5F). In comparison to the parental strain, the survival of Δ*vapBC26* mutant strain was marginally reduced by ~3.0-fold upon exposure to oxidative stress for either 24 h or 72 h (Fig. 5F). We also demonstrate that the increased susceptibility of Δ*vapBC13* and Δ*vapBC26* mutant strains was partially restored by 2.0-fold in complemented strains upon exposure to oxidative stress for 72 h (Fig. 5C, F). As shown in Supplementary Fig. S7A–L, the survival of Δ*vapC13*, Δ*vapBC13*, Δ*vapC26*, and Δ*vapBC26* was comparable to that of wild type strain after exposure to other stress conditions such as nitrosative, nutritional or detergent stress. Taken together, our results suggest that, except for oxidative stress, VapBC13 and VapBC26 TA systems are dispensable for the survival of *M. tuberculosis* upon exposure to the other stress conditions investigated in the present study.

VapBC13 and VapBC26 TA systems are dispensable for *M. tuberculosis* survival under antibiotic stress

TA systems have been postulated to be involved in antibiotic persistence[16,92]. Antibiotic persistence is a significant challenge in treating bacterial infections, as persistent bacteria are responsible for disease relapse. Several

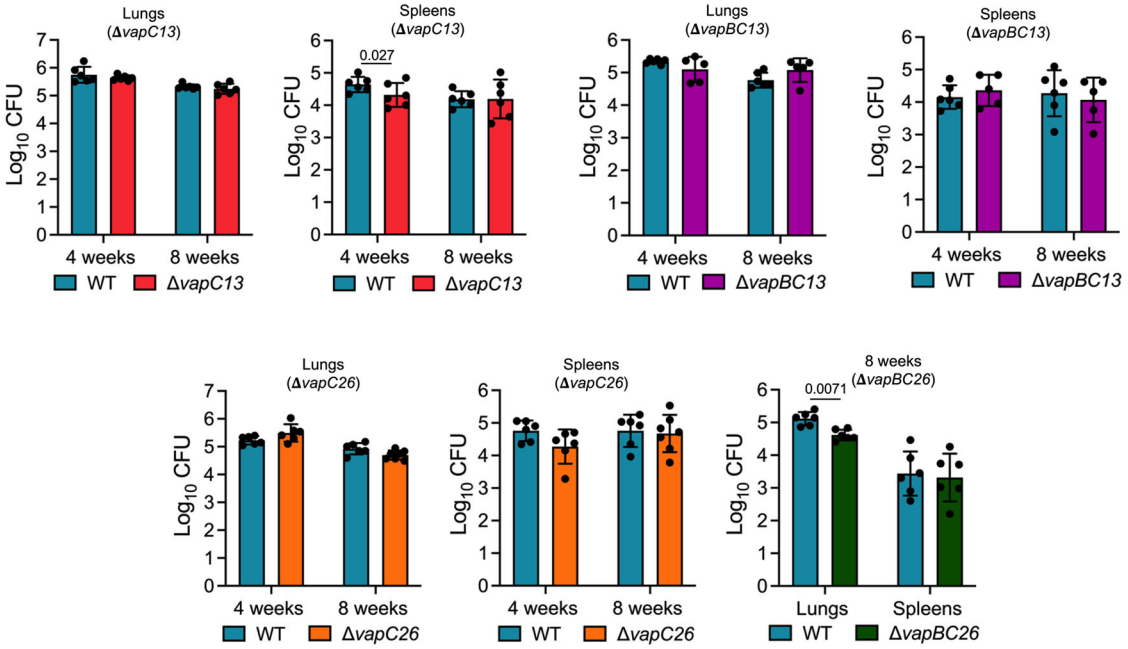

Fig. 6 | In vivo survival of parental and various mutant strains of *M. tuberculosis* in guinea pigs. The bacterial loads in the lungs and spleens of guinea pigs infected with various strains were determined at either 4 weeks or 8 weeks post-infection. The data shown in these panels is the mean ± SD of $\log_{10}$ CFU obtained from either 5 or 6 guinea pigs per strain per time point. *P values* depicted on the graphs were assessed using a two-tailed paired t-test. Source data is provided in Supplementary Data Set 4.

studies have shown that toxins belonging to type II TA systems, such as MqsR, TisB, MazF, RelE, YafQ and YoeB are involved in persister formation after exposure to either ampicillin or ciprofloxacin or tobramycin[16,92–94]. However, the contribution of TA systems to antibiotic-mediated persistence is debatable as the simultaneous deletion of 10 TA systems in *E. coli* does not affect persister cell formation[6,95]. We have previously reported that simultaneous deletion of MazF3, MazF6 and MazF9 increases the susceptibility of *M. tuberculosis* upon exposure to levofloxacin[38]. The overexpression of VapC21 has also been shown to increase the survival of *M. smegmatis* after exposure to aminoglycosides[53]. It has also been reported that overexpression of *M. tuberculosis* RelE homologue increases the persister formation upon exposure to rifampin, ofloxacin, isoniazid and gentamycin in *M. tuberculosis*[54,96]. We also demonstrated that VapBC3, VapBC4, VapC28, VapBC11, VapC22 or MenT2 or MenT3 and MenT4 do not contribute to antibiotic susceptibility of *M. tuberculosis* in vitro[17,25,37,50,51]. In the present study, we also evaluated the contribution of VapBC13 and VapBC26 in antibiotic-mediated persistence. For these experiments, mid-log phase cultures of various strains were exposed to drugs with different mechanisms of action, such as isoniazid, rifampicin and levofloxacin. As shown in Supplementary Fig. S7M–P, the survival of Δ*vapC13*, Δ*vapBC13*, Δ*vapC26*, and Δ*vapBC26* was comparable to the survival of parental strain upon exposure to these drugs. This data suggests that distantly related VapBC13 and VapBC26 TA pairs are not essential for *M. tuberculosis* survival in the presence of drugs.

VapBC13 and VapBC26 TA systems are dispensable for *M. tuberculosis* pathogenesis

The presence of a large number of TA systems suggests that metabolic shutdown associated with the activation of toxins belonging to type II TA systems might enable *M. tuberculosis* to persist in host tissues. Previously, we have reported that *M. tuberculosis* strains with a deletion in either *mazF3*, *mazF6* and *mazF9*, *vapBC11*, *vapBC3*, *vapBC4*, *vapC22*, *higB1*, *menT2* or *menT3* and *menT4* impaired the growth of *M. tuberculosis* in guinea pigs[17,25,37,38,49–51]. The growth patterns of Δ*vapC21*, Δ*vapC28* or Δ*darTG* deletion strains were comparable with parental strain in the lungs and spleens of infected animals[37,52,53]. In the present study, we compared the in vivo phenotype of parental, Δ*vapC13*, Δ*vapBC13*, Δ*vapC26 and* Δ*vapBC26* strains using a guinea pig model of infection. The bacterial loads in the lungs of guinea pigs infected with either parental, Δ*vapC13*, Δ*vapBC13* or Δ*vapC26* strains were comparable at 4 weeks post-infection (Fig. 6). In the case of spleens, the bacillary loads were comparable in guinea pigs infected with parental, Δ*vapBC13* or Δ*vapC26* strain (Fig. 6). However, at 4 weeks post-infection, the bacterial burdens in the spleens of Δ*vapC13* mutant strain infected guinea pigs were marginally reduced by 2.6-fold in comparison to guinea pigs infected with the parental strain (Fig. 6). As shown in Fig. 6, lungs and splenic bacillary loads were comparable in guinea pigs infected with either parental, Δ*vapC13*, Δ*vapBC13* or Δ*vapC26* at 8 weeks post-infection. However, we observed the lung bacillary loads in guinea pigs infected with Δ*vapBC26* were marginally reduced by 3.0-fold in comparison to parental strain-infected guinea pigs at 8 weeks post-infection (Fig. 6). We did not observe any significant difference in splenic bacillary loads of guinea pigs infected with either wild type or Δ*vapBC26* at 8 weeks post-infection (Fig. 6). The extent of disease progression was also determined by histopathology analysis. As shown in Supplementary Fig. S8, similar lung damage and alveolar space were observed in lung sections of guinea pigs infected with various strains at both time points. These observations suggest that despite being more susceptible upon exposure to oxidative stress in vitro, the growth patterns of these mutant strains were comparable to the parental strain in aerosol infected guinea pigs.

Discussion

TA systems are small genetic entities that encode for a toxin protein, which inhibits bacterial growth, and an antitoxin, which neutralizes the toxin. TA systems are abundantly present in bacterial genomes and are involved in diverse physiological processes such as plasmid maintenance and phage defence[7,8,97]. However, their exact roles in bacterial stress adaptation and virulence have not been studied comprehensively. *M. tuberculosis* genome encodes for ~90 TA pairs, the majority of which belong to the VapBC subfamily. The VapC toxins belonging to the VapBC subfamily are ribonucleases that upon overexpression inhibit bacterial growth mostly in a bacteriostatic manner[22,33,37,98]. It has been reported that ectopic expression of toxins results in significant changes in transcriptional profiles of *M. tuberculosis*, and these are similar to the profiles obtained upon exposure of *M. tuberculosis* to EHR, nutritional or oxidative stress. TA systems regulate

bacterial growth and have been hypothesized as metabolic stress managers that might contribute in a cumulative manner to bacterial physiology and pathogenesis[4,9,99,100]. The paralogous expansion of *M. tuberculosis* TA systems also indicates that these systems might have evolved to promote the intracellular survival of the bacilli[11,32,33]. A better understanding of the functions of TA systems could lead to the development of new strategies to combat bacterial infections.

Previously, through comprehensive bioinformatics and phylogenetic analysis, toxins and antitoxins belonging to the VapBC family have been categorized into paralogous subclusters[11]. While VapC13 was grouped into subcluster I, VapB13, VapC26, and VapB26 were designated as orphans, highlighting their distant relationship with other homologues[11]. In the present study, we have performed experiments to investigate the role of distantly related VapBC13 and VapBC26 TA systems in *M. tuberculosis* pathophysiology. We show that expression of VapC13 or VapC26 inhibited *M. tuberculosis* growth in agreement with earlier studies[37]. Previous studies have shown that *M. tuberculosis* VapC toxins mostly have two distinct RNA targets: tRNA or 23S rRNA[22,43,45]. VapC26 has been shown to cleave SRL of 23S rRNA, whereas the cellular target of VapC13 has not been determined so far[22]. The detailed analysis of RNA-Seq data revealed that in comparison to the parental strain, the protection ratios for several tRNAs were significantly reduced in VapC13 and VapC26 overexpression strains. Using ribonuclease assays, we confirmed in vitro degradation of *serT* and *leuW* by the purified MBP-VapC13 and MBP-VapC26 proteins, respectively. We observed that the protection ratios dropped around 10-25 nucleotides in potential tRNA targets for VapC13 and VapC26. We speculate that this drop in protection ratios might be due to multiple cleavage sites or exposure of loop-structured resides to exonucleases following VapC-mediated cleavage of their potential tRNA targets[101,102]. Future experiments will include performing 3'-end sequencing of total RNA isolated from VapC13 and VapC26 overexpression strains to determine other cellular targets of VapC13 and VapC26 in their native host, as reported in other studies[101,103]. Also, despite performing rRNA depletion before the synthesis and sequencing of cDNA libraries, we observed that few sequencing reads mapped to rRNA. Since rRNA is highly abundant, rRNA depletion was incomplete in our experiment. Thus, we further analysed these sequenced rRNA reads to determine protection ratios of 23S and 16S rRNA in parental, VapC13 overexpression and VapC26 overexpression strains. The 23S and 16S rRNA profiles were comparable in parental, VapC13 overexpression and VapC26 overexpression strains of *M. tuberculosis*. These observations are inconsistent with an earlier study, where VapC26 has been shown to cleave the SRL of the 23S rRNA[22]. This might be attributed to the levels of free VapC26 toxin and different host strains used in our and previous study[22].

RNA-Seq experiments revealed that overexpression of VapC13 or VapC26 significantly altered the transcriptome that encodes for 30% and 5% of the *M. tuberculosis* proteome, respectively. The ectopic expression of free VapC13 or VapC26 resulted in increased transcript levels of genes encoding for either ribosomal or regulatory proteins or proteins involved in translation processes. Similar transcriptional profiles have also been observed upon overexpression of either VapC22, VapC21, VapC11 or MazF6 in *M. tuberculosis*[17,25,53,57]. The presence of free VapC13 also reduced the transcript levels for proteins involved in lipid synthesis or their transport to the cell envelope. The levels of transcript encoding for proteins belonging to the PE_PGRS family were significantly reduced in the VapC26 overexpression strain. Several studies have shown that PE_PGRS family proteins encode for cell wall-associated antigens and are involved in nutrient uptake and disease pathogenesis[78,104,105]. It has been previously reported that the frequency of the occurrence of leucine residues is ~6% in PE-PGRS family proteins in *M. tuberculosis*[106]. We hypothesize that overexpression of the VapC26 toxin results in reduced incorporation of *leuW* tRNA, ribosome stalling, and regulation of the transcripts encoding for leucine-rich proteins, including PE_PGRS family proteins. Identification of regulatory proteins as hub nodes in the top response network of VapC13 and VapC26 overexpression strains also explains the large-scale changes observed in the expression profiles of these strains. The increased expression of ribosomal proteins in toxin overexpression strains can be attributed to possible ribosomal stalling mediated by the ribonuclease activity of the free toxins, as reported earlier[18,107]. The decreased levels of transcripts encoding for proteins involved in either ATP synthesis, intermediary metabolism or lipid metabolism indicate that the metabolism of *M. tuberculosis* is significantly reduced upon VapC13 or VapC26 overexpression. This reduced metabolism might enable bacteria to escape from the host or antibiotics-derived stress environments to facilitate their long-term survival inside the host[108–110]. The levels of transcripts encoding for proteins involved in oxidative stress were also increased in VapC13 and VapC26 overexpression strains. This suggests that the presence of free toxins results in increased expression of stress-responsive genes that might enable *M. tuberculosis* to adapt inside host tissues to establish long-term persistent infection. Further, we also observed that ectopic expression of either VapC13 or VapC26 results in the activation of canonical and non-canonical TA pairs in *M. tuberculosis*. This activation might result from a possible positive feedback loop mechanism between TA systems, as suggested earlier for *E. coli* and *M. tuberculosis*[37,79,111]. We hypothesize that other tRNAs with lower protection ratios are either the cellular targets of VapC13 or VapC26 or the non-cognate toxins whose expression was increased in these overexpression strains.

In order to investigate the role of VapBC13 and VapBC26 TA systems in *M. tuberculosis* pathophysiology, we constructed toxin deficient (Δ*vapC13*, Δ*vapC26*) and TA system deficient (Δ*vapBC13* and Δ*vapBC36*) deletion strains. The growth characteristics of parental and mutant strains were comparable in both liquid and solid mediums. Amongst the various stress conditions tested, we noticed that compared to the wild type strain, Δ*vapC13*, Δ*vapBC13* and Δ*vapBC26* strains were mildly susceptible to killing upon exposure to oxidative stress. The survival of wild type and Δ*vapC26* strains was comparable in these stress conditions. This increased susceptibility of Δ*vapC13*, Δ*vapBC13* and Δ*vapBC26* strains upon exposure to oxidative stress was partially restored in their respective complemented strains. The vector integration at the *attB* site may be the possible reason for the partial complementation in the complemented strains, which could result in a lack of optimal transcription from the *hsp65* promoter. We also speculate that deletion of these TA pairs from the genome of *M. tuberculosis* might have additional consequences upon exposure to oxidative stress that may not be easily evident from endpoint CFU measurements and would require additional future experiments. Previous studies have shown that relative to the *M. tuberculosis* parental strain, strains harbouring deletions in either *ndH* or *ndH* and *nuoAN* or Rv2159c or Rv2745c or *katG* or *vapBC11* or *vapC22* or *mazF3*, *mazF6* and *mazF9* or *menT3* and *menT4* were more susceptible to killing upon exposure to oxidative stress and also attenuated for growth in vivo[17,25,38,51,112–115]. Interestingly, despite being susceptible to killing upon exposure to oxidative stress, we observed that the growth patterns of wild type and these mutant strains were almost comparable in the lungs and spleens of guinea pigs during both acute and chronic stages of infection. These observations suggest that functional redundancy might exist between TA systems in *M. tuberculosis*, and a subset of these might function cumulatively in vivo. The development of a strain with simultaneous deletion in multiple TA systems will further aid in comprehending the role of these TA modules in the physiology and pathogenesis of *M. tuberculosis*. In conclusion, we have performed experiments to delineate the contribution of VapBC13 and VapBC26 in stress adaptation and pathogenesis of *M. tuberculosis*.

Material and methods

Bacterial strains and culture conditions

The details of plasmids and strains used in this study are shown in Table 2. Unless mentioned, all the chemicals, reagents and oligos were purchased from Sigma Aldrich and Merck. HB-101 and XL-1 blue strains of *E. coli* were used for cloning purposes. *E. coli* strains were cultured in either LB broth or LB agar at 37 °C, 200 rpm. *M. tuberculosis* (H_{37}Rv strain) and *M. smegmatis* ($mc^2$155 strain) were cultured in Middlebrook 7H9 or 7H11 medium

Table 2 | Description of the plasmids and strains used in this study

Strain Name	Description	Source
E. coli XL1 Blue	*recA1 endA1 gyrA96 thi-1 hsdR17 supE44 relA1 lac [F' proAB lacIq* ZΔM15 Tn10 (Tet^r)].	Stratagene, USA
E. coli HB101	*F$^-$, thi^{-1}, hsdS20 (r_B- m_B), supE44, recA13, ara-14, leuB6, proA2, lacY1, galK2, rpsL20 (strr), xyl-5, mtl-1*.	Promega, USA
E. coli BL-21 (λDE3, pLysE)	*F–, ompT, hsdS_B (r_B–, m_B–), dcm, gal, λ(DE3), pLysE, Cm^r*	Promega, USA
M. tuberculosis H_{37}Rv	Virulent strain of *M. tuberculosis*.	ATCC27294
M. smegmatis mc^{2}155	Non-pathogenic fast growing mycobacteria	A kind gift from Prof. Anil K Tyagi
Δ*vapC13*	Rv1838c mutant strain of *M. tuberculosis*.	This work
Δ*vapBC13*	Rv1838c-Rv1839c mutant strain of *M. tuberculosis*.	This work
Δ*vapC26*	Rv0582 mutant strain of *M. tuberculosis*.	This work
Δ*vapBC26*	Rv0581-Rv0582 mutant strain of *M. tuberculosis*.	This work
Δ*vapC13-CT*	Δ*vapC13* strain of *M. tuberculosis* complemented with Rv1838c.	This work
Δ*vapBC13-CT*	Δ*vapBC13* strain of *M. tuberculosis* complemented with Rv1838c-Rv1839c.	This work
Δ*vapBC13*::*vapC13^{OE}*	Δ*vapBC13* strain of *M. tuberculosis* harbouring anhydrotetracycline-inducible tagged vector, pTetR-int-*vapC13*.	This work
Δ*vapC26-CT*	Δ*vapC26* strain of *M. tuberculosis* complemented with Rv0582.	This work
Δ*vapBC26-CT*	Δ*vapBC26* strain of *M. tuberculosis* complemented with Rv0581-Rv0582.	This work
Δ*vapBC26*::*vapC26^{OE}*	Δ*vapBC26* strain of *M. tuberculosis* harbouring anhydrotetracycline-inducible tagged vector, pTetR-int-*vapC26*.	This work
H37Rv, pTetR	*M. tuberculosis* harbouring anhydrotetracycline-inducible vector, pTetR.	37
H37Rv, pTetR-*vapC13*	*M. tuberculosis* harbouring anhydrotetracycline-inducible vector, pTetR-*vapC13*.	37
H37Rv, pTetR-*vapC26*	*M. tuberculosis* harbouring anhydrotetracycline-inducible vector, pTetR-*vapC26*.	37
mc^{2}155, pTetR- *myc*	*M. smegmatis* strain harbouring anhydrotetracycline-inducible *myc* tagged vector, pTetR-*myc*.	This work
mc^{2}155, pTetR-*vapC13 myc*	*M. smegmatis* strain harbouring anhydrotetracycline-inducible *myc* tagged vector, pTetR-*vapC13 myc*.	This work
mc^{2}155, pTetR-*vapC26 myc*	*M. smegmatis strain* harbouring anhydrotetracycline-inducible *myc* tagged vector, pTetR-*vapC26 myc*.	This work
Plasmid name	**Description**	**Source**
pGEM-T easy	T/A cloning vector, amp^r	Promega, UK
pYUB854	Cloning vector, hyg^r	117
pYUB854Δ*vapC13::hyg^r*	pYUB854 with Rv1838c upstream and downstream region flanking the hygromycin resistance gene.	This work
pYUB854Δ*vapBC13::hyg^r*	pYUB854 with Rv1839c upstream and Rv1838c downstream region flanking the hygromycin resistance gene.	This work
pYUB854Δ*vapC26::hyg^r*	pYUB854 with Rv0582 upstream and downstream region flanking the hygromycin resistance gene.	This work
pYUB854Δ*vapBC26::hyg^r*	pYUB854 with Rv0581 upstream and Rv0582 downstream region flanking the hygromycin resistance gene.	This work
pMAL-c2x	Prokaryotic expression vector with MBP tag at amino-terminus.	New England Biolabs, US
pMAL-c2x-*vapC13*	pMAL-c2x harbouring Rv1838c.	This work
pLimo	Prokaryotic expression vector with MBP tag at amino-terminus.	120
pLimo-*vapC26*	pLimo harbouring Rv0582.	This work
pTetR	anhydrotetracycline inducible vector system.	116
pTetR-*myc*	anhydrotetracycline inducible vector system with *myc* tag at C-terminal.	This work
pTetR-int	anhydrotetracycline inducible vector system.	37
pTetR-*vapC13*	pTetR vector harbouring Rv1838c.	37
pTetR-*vapC13 myc*	pTetR-*myc* vector harbouring Rv1838c.	This work
pTetR-int-*vapC13*	pTetR-int vector harbouring Rv1838c.	This work
pTetR-v*apC26*	pTetR vector harbouring Rv0582.	37
pTetR-*vapC26 myc*	pTetR-*myc* vector harbouring Rv0582.	This work
pTetR-int-*vapC26*	pTetR-int vector harbouring Rv0582.	This work
pJEB402	Constitutive mycobacterial expression integrative vector.	A kind gift from Dr Amit Kumar Pandey
pJEB402-*vapBC13*	pJEB402 harbouring Rv1838c-Rv1839c.	This work
pJEB402-*vapBC26*	pJEB402 harbouring Rv0581-Rv0582.	This work

Table 2 (continued) | Description of the plasmids and strains used in this study

Strain Name	Description	Source
pYUB159	temperature sensitive mycobacteriophage	117
pYUB159Δ*vapC13::hyg*^{r}	pYUB159 derivative to replace Rv1838c with hygromycin resistance gene in *M. tuberculosis*.	This work
pYUB159Δ*vapBC13::hyg*^{r}	pYUB159 derivative to replace Rv1838c-Rv1839c with hygromycin resistance gene in *M. tuberculosis*.	This work
pYUB159Δ*vapC26::hyg*^{r}	pYUB159 derivative to replace Rv0582 with hygromycin resistance gene in *M. tuberculosis*.	This work
pYUB159Δ*vapBC26::hyg*^{r}	pYUB159 derivative to replace Rv0581-Rv0582 with hygromycin resistance gene in *M. tuberculosis*.	This work

supplemented with either 1× ADS or 1× OADS, respectively, at 37 °C, 150 rpm as described earlier[49,53]. In *E. coli*, ampicillin (50 µg/ml), kanamycin (25 µg/ml), tetracycline (10 µg/ml) and hygromycin (150 µg/ml, Invitrogen) were added when required. For mycobacterial culturing, hygromycin and kanamycin were added at 50 µg/ml and 25 µg/ml, respectively.

Generation of various overexpression, knockout and complemented strains

The details of primers used in the study are shown in Supplementary Table S1. For overexpression studies, *vapC13* or *vapC26* were amplified by PCR and cloned in the anhydrotetracycline (Atc) inducible vector, pTetR, pTetR-*myc* or pTetR-int as per standard protocols[37,116]. *M. tuberculosis* strains harbouring deletions in either *vapC13*, *vapBC13*, *vapC26* or *vapBC26* were constructed via homologous recombination using temperature-sensitive mycobacteriophages as described earlier[117]. Briefly, 800 base pairs of upstream and downstream regions of either *vapC13*, *vapBC13*, *vapC26 or vapBC26* were cloned in pYUB854 flanking the hygromycin cassette. The recombinant cosmids were *Pac* I digested and packaged into phagemid pYUB159. The recombinant phagemid was electroporated into *M. smegmatis* to generate high-titre mycobacteriophages. The mutant strains were generated by transducing mid-log phase cultures of *M. tuberculosis* $H_{37}Rv$ (OD_{600nm} ~ 0.8) using high-titre temperature-sensitive mycobacteriophages. The replacement of either *vapC13*, *vapC26*, *vapBC13* or *vapBC26* with the hygromycin resistance gene in their respective mutant strains was verified by Southern blot. For the generation of the complementation strains, *vapBC13* or *vapBC26* were PCR amplified and cloned in an integrative vector, pJEB402, under the transcriptional control of the *hsp65* promoter. The recombinant plasmids were electroporated in their respective mutant strains, and transformants were selected on 7H11 plates supplemented with hygromycin and kanamycin.

In vitro growth, stress and drug susceptibility experiments

For growth patterns of overexpression strains, early log phase cultures (OD_{600nm} ~ 0.2) were induced by adding 50 ng/ml Atc. The effect of overexpression of VapC13 and VapC26 on *M. smegmatis* and *M. tuberculosis* growth was determined by measuring OD_{600nm} at regular intervals till the stationary phase was attained. In order to determine the expression levels of myc-tagged toxins, recombinant *M. smegmatis* overexpression strains were lysed by bead beating and clarified lysates were prepared as per standard protocols. The expression of myc-tagged toxins in clarified lysates was determined using anti-myc antibodies (Cell signaling technology) as per the manufacturer's recommendations. The growth patterns of parental and mutant strains were compared by measuring OD_{600nm} till the stationary phase was attained. The growth curves were performed using a 10 ml culture volume in 50 ml sterile polypropylene conical tubes. For biofilm experiments, mid-log phase cultures of various strains were harvested and washed twice with Sauton's medium (0.5 g/l aspartate, 1.0 g/l KH_2PO_4, 2.5 g/l Na_2HPO_4, 50 mg/l ferric ammonium citrate, 0.05 g/l $MgSO_4$.7H2O, 0.05 g/l $CaCl_2$ and 0.01 g/l $ZnSO_4$). Subsequently, washed cultures were diluted and added to 6 well plates, sealed with parafilm and incubated at 37 °C for 3–4 weeks without shaking. The susceptibility of various *M. tuberculosis* strains upon exposure to either oxidative, nitrosative, nutritional, cell wall stress or drugs was determined as described previously[37,38]. For bacterial enumeration, at designated time points, 10.0-fold serial dilutions were prepared and plated on MB 7H11 medium at 37 °C for 3-4 weeks.

In vitro transcriptomics, data curation and analysis

RNA-Seq experiments were performed to determine the effect of VapC13 and VapC26 overexpression on transcription profiles of *M. tuberculosis*. For RNA-Seq experiments, early-log phase cultures (OD_{600nm} ~ 0.2–0.3) of *M. tuberculosis* strains harbouring either pTetR or pTetR-*vapC13* or pTetR-*vapC26* were induced with the addition of 50 ng/ml Atc for 24 h. For total RNA isolation, induced cultures were harvested by centrifugation, washed twice with 1× PBS and lysed by bead beating in Trizol (Ambion, Inc). Total RNA was extracted by phenol-chloroform, precipitated with isopropanol and eluted using Qiagen RNA isolation kit as per the manufacturer's instructions. The extracted RNA was subsequently subjected to DNase I treatment, rRNA depletion and cDNA library was prepared. The integrity of the DNase-treated RNA was checked on the 1% agarose gel. The cDNA library was sequenced using the Illumina His seq platform at MedGenome Pvt. Ltd. Subsequently, the quality of raw data obtained from the control and overexpression strain was assessed using FastQC v0.11.4. The reference *M. tuberculosis* H37Rv genome was downloaded from the ENSEMBL database, indexed using Bowtie2, and aligned to the reference genome with TopHat v2.1.1. The transcripts were assembled using Cufflinks v2.2.1 and merged into a cohesive set using Cuffmerge. The Cuffdiff output of gene counts was analysed for differential gene expression using the CummeRbund (R-package) software.

Network analysis and tRNA cleavage site prediction

MtbPPIN (*M. tuberculosis* protein-protein interaction network) is a complex directed graph of the genome-wide interconnections between proteins in *M. tuberculosis*. A condition-specific PPI network was generated by integrating gene expression data onto the database MtbPPIN in the form of weights to the nodes and edges. The node weight for gene *i* (NWi) was calculated using Eq. (1) as described previously[57].

$$NW_i = |T_i - C_i| \tag{1}$$

Here, T_i and C_i are the gene expression of gene *i* in the test condition and control condition, respectively. Edge weights ($EW_{i,j}$) between the interacting nodes *i* and *j* were then calculated using the following Eqs. (2) and (3):

$$EW_i = NW_i * NW_j \tag{2}$$

$$EW'_{i,j} = \left(EW_{\max} + EW_{\min}\right) - EW_{ij} \tag{3}$$

Here, NW_i and NW_j are the node weights of the edge-forming interacting nodes, EW_{max} and EW_{min} are the maximum and minimum edge weights of the entire network, respectively, and EW'_{ij} is the inversed Edge weight. A sensitive network mining algorithm was used to identify perturbations in the given condition. It computes all-to-all shortest paths in the weighted network using Djikstra's algorithm, computes path scores by taking the summation of all edge scores, normalizes and ranks them to identify the most perturbed paths. A stringent threshold was used to capture

the top ~500 genes from the network. The generated response networks were visualized using Cytoscape 3.7.1.

Further, SAMtools depth was used to calculate the per-base coverage individually for all replicates in both control and overexpressed conditions[118]. The per-base counts were further normalized by dividing counts at each nucleotide position by the total count of that replicate and multiplying by the *M. tuberculosis* genome size (Eq. (4)).

$$normalized_{count_i} = \frac{count_i}{\sum count_i} \times 4.4 \times 10^6 \quad (4)$$

where i is the replicate number.

The normalized count average across the triplicates was performed at each position individually for both conditions (Eq. (5)). This was further used to calculate the protection ratio. The ratio at each nucleotide position was calculated as the $\log_2$ transformed toxin overexpression: control ratio (Eq. (6)).

$$normalized_{count_{avg}} = \frac{\sum normalized_{count_i}}{number\ of\ replicates} \quad (5)$$

$$\text{Protection ratio} = \log_2\left(\frac{normalised_{count\,avg}(OE)}{normalised_{count\,avg}(control)}\right) \quad (6)$$

In vitro transcription and tRNA cleavage assays

For protein purification, genes encoding for VapC13 or VapC26 were amplified by PCR and cloned into pMALc2x or pLimo vectors, respectively. The recombinant plasmids were transformed into BL21 (λDE3), pLysE for protein expression studies. The recombinant strains were cultured in TB medium till OD_{600nm} ~ 0.6, and expression of MBP-tagged proteins was induced by adding 1.0 mM isopropyl β-D-1-thiogalactopyranoside. The recombinant proteins were purified by affinity chromatography using amylose resin (New England Biolabs) as per the manufacturer's recommendations. The purified protein fractions were dialysed, concentrated and stored in protein elution buffer (20 mM Tris-Cl, pH-8.0, 200 mM NaCl, 1% glycerol containing protease inhibitor tablet). For in vitro transcription, oligonucleotides (with T7 overhang in the forward primer) encoding for various tRNA sequences were synthesized and annealed as per standard protocols. Next, using these annealed oligos, PCR amplification was performed using the T7 promoter and a second primer corresponding to the 3' end of the tRNA gene. In vitro transcription for tRNA molecules was performed using gel purified PCR product and T7 RNA polymerase (Takara Bio Inc) as per manufacturer recommendations. The tRNA preparation was *Dnase* I treated, ammonium acetate precipitated and resuspended in nuclease free water. For in vitro tRNA cleavage assays, *Dnase* I treated tRNA preparations were incubated with either 10 μM of purified MBP or MBP-tagged toxins in 1× cleavage buffer (20 mM Tris-Cl, pH-7.4, 60 mM NaCl, 1 mM DTT and 10 mM MgCl2) at 37 °C for 1 h. The reactions were inactivated by adding 1× RNA formamide dye and resolved on 15% UREA-PAGE as per standard protocols[25].

Animal experiments

The Institutional Animal Ethics Committee of the Translational Health Science and Technology Institute approved the use of animals in these experiments (Approval ID- THSTI/IAEC/106). The guidelines of the Committee for Control and Supervision of Experiments on Animals (CCSEA, Govt. of India) were followed to perform the animal experiments. For aerosol infection, mid-log phase cultures (OD_{600nm} ~ 0.8) of various strains were harvested, washed twice with 1× PBS and single-cell suspensions were prepared in normal saline. Subsequently, 6–8 weeks-old female guinea pigs (Dunkin Hartley strain) were exposed to aerosol infection using the inhalation exposure system (Glascol) as per standard protocols. The extent of disease progression was evaluated by determining bacterial loads and tissue damage in guinea pigs at either 4 or 8 weeks post-infection. For bacterial enumeration, lungs and spleens were homogenized in 2 ml of normal saline and 10.0-fold serial dilutions were plated on MB 7H11 agar plates. For histopathology analysis, a portion of the lung was fixed in formalin, paraffin embedded and stained with haematoxylin and eosin. The images of H&E-stained sections of infected lung tissues were analysed by an experienced pathologist.

Statistical analysis and data reproducibility

Graph Pad Prism 9.1.1 software (GraphPad Software Inc., CA, USA) was used for the preparation of graphs and statistical analysis. The *P value* of <0.05 was considered to be statistically significant. The number of replicates and statistical tests used are mentioned in the respective figure legends.

Reporting summary

Further information on research design is available in the Nature Portfolio Reporting Summary linked to this article.

Data availability

The published article and its supplementary information include all the data generated and analysed in this study. The RNA-Seq data discussed in the present study have been deposited in NCBI's Gene Expression Omnibus and is accessible through either GEO Series accession number GSE237792 or Bioproject PRJNA996620 (*M. tuberculosis*) (https://www.ncbi.nlm.nih.gov/bioproject/PRJNA996620)[119]. All the source values underlying all figures and the uncropped and unedited blots are available in supplementary data set 4. A description of the additional supplementary data files is provided along with this manuscript.

Received: 28 August 2023; Accepted: 1 October 2024;
Published online: 30 October 2024

References

1. Hayes, F. Toxins-antitoxins: plasmid maintenance, programmed cell death, and cell cycle arrest. *Science* **301**, 1496–1499 (2003).
2. Ogura, T. & Hiraga, S. Mini-F plasmid genes that couple host cell division to plasmid proliferation. *Proc. Natl Acad. Sci. USA* **80**, 4784–4788 (1983).
3. Unterholzner, S. J., Poppenberger, B. & Rozhon, W. Toxin-antitoxin systems: Biology, identification, and application. *Mob. Genet Elem.* **3**, e26219 (2013).
4. Harms, A., Brodersen, D. E., Mitarai, N. & Gerdes, K. Toxins, Targets, and Triggers: An Overview of Toxin-Antitoxin Biology. *Mol. Cell* **70**, 768–784 (2018).
5. Hayes, F. & Van Melderen, L. Toxins-antitoxins: diversity, evolution and function. *Crit. Rev. Biochem Mol. Biol.* **46**, 386–408 (2011).
6. Fraikin N., Goormaghtigh F., Van Melderen L. Type II Toxin-Antitoxin Systems: Evolution and Revolutions. *J Bacteriol* **202**, (2020).
7. Jurenas, D., Fraikin, N., Goormaghtigh, F. & Van Melderen, L. Biology and evolution of bacterial toxin-antitoxin systems. *Nat. Rev. Microbiol* **20**, 335–350 (2022).
8. Qiu, J., Zhai, Y., Wei, M., Zheng, C. & Jiao, X. Toxin-antitoxin systems: Classification, biological roles, and applications. *Microbiol Res* **264**, 127159 (2022).
9. Page, R. & Peti, W. Toxin-antitoxin systems in bacterial growth arrest and persistence. *Nat. Chem. Biol.* **12**, 208–214 (2016).
10. Akarsu, H. et al. TASmania: A bacterial Toxin-Antitoxin Systems database. *PLoS Comput Biol.* **15**, e1006946 (2019).
11. Tandon, H. et al. Bioinformatic and mutational studies of related toxin-antitoxin pairs in Mycobacterium tuberculosis predict and identify key functional residues. *J. Biol. Chem.* **294**, 9048–9063 (2019).
12. Diaz-Orejas, R., Espinosa, M. & Yeo, C. C. The Importance of the Expendable: Toxin-Antitoxin Genes in Plasmids and Chromosomes. *Front Microbiol* **8**, 1479 (2017).

13. LeRoux, M. & Laub, M. T. Toxin-Antitoxin Systems as Phage Defense Elements. *Annu Rev. Microbiol* **76**, 21–43 (2022).
14. Song, S. & Wood, T. K. A Primary Physiological Role of Toxin/Antitoxin Systems Is Phage Inhibition. *Front Microbiol* **11**, 1895 (2020).
15. Ronneau, S. & Helaine, S. Clarifying the Link between Toxin-Antitoxin Modules and Bacterial Persistence. *J. Mol. Biol.* **431**, 3462–3471 (2019).
16. Wang, X. & Wood, T. K. Toxin-antitoxin systems influence biofilm and persister cell formation and the general stress response. *Appl Environ. Microbiol* **77**, 5577–5583 (2011).
17. Agarwal, S. et al. VapBC22 toxin-antitoxin system from Mycobacterium tuberculosis is required for pathogenesis and modulation of host immune response. *Sci. Adv.* **6**, eaba6944 (2020).
18. Barth, V. C. et al. Mycobacterium tuberculosis VapC4 toxin engages small ORFs to initiate an integrated oxidative and copper stress response. *Proc. Natl Acad. Sci. USA* **118**, e2022136118 (2021).
19. Cai, T. et al. HigBA toxin-antitoxin system of Weissella cibaria is involved in response to the bile salt stress. *J. Sci. Food Agric* **102**, 6749–6756 (2022).
20. Moreno-Del Alamo, M., Tabone, M., Lioy, V. S. & Alonso, J. C. Toxin zeta Triggers a Survival Response to Cope with Stress and Persistence. *Front Microbiol* **8**, 1130 (2017).
21. Han, Y. & Lee, E. J. Substrate specificity of bacterial endoribonuclease toxins. *BMB Rep.* **53**, 611–621 (2020).
22. Winther, K., Tree, J. J., Tollervey, D. & Gerdes, K. VapCs of Mycobacterium tuberculosis cleave RNAs essential for translation. *Nucleic Acids Res* **44**, 9860–9871 (2016).
23. Kurata, T. et al. A hyperpromiscuous antitoxin protein domain for the neutralization of diverse toxin domains. *Proc. Natl Acad. Sci. USA* **119**, e2102212119 (2022).
24. Mansour, M. et al. Substrate recognition and cryo-EM structure of the ribosome-bound TAC toxin of Mycobacterium tuberculosis. *Nat. Commun.* **13**, 2641 (2022).
25. Deep, A. et al. Structural, functional and biological insights into the role of Mycobacterium tuberculosis VapBC11 toxin-antitoxin system: targeting a tRNase to tackle mycobacterial adaptation. *Nucleic Acids Res* **46**, 11639–11655 (2018).
26. Schifano, J. M. et al. Mycobacterial toxin MazF-mt6 inhibits translation through cleavage of 23S rRNA at the ribosomal A site. *Proc. Natl Acad. Sci. USA* **110**, 8501–8506 (2013).
27. Walling, L. R. & Butler, J. S. Toxins targeting transfer RNAs: Translation inhibition by bacterial toxin-antitoxin systems. *Wiley Interdiscip. Rev. RNA* **10**, e1506 (2019).
28. Rocker, A. et al. The ng_zeta1 toxin of the gonococcal epsilon/zeta toxin/antitoxin system drains precursors for cell wall synthesis. *Nat. Commun.* **9**, 1686 (2018).
29. Jurenas, D., Garcia-Pino, A. & Van Melderen, L. Novel toxins from type II toxin-antitoxin systems with acetyltransferase activity. *Plasmid* **93**, 30–35 (2017).
30. Goeders, N. & Van Melderen, L. Toxin-antitoxin systems as multilevel interaction systems. *Toxins (Basel)* **6**, 304–324 (2014).
31. Singh, G., Yadav, M., Ghosh, C. & Rathore, J. S. Bacterial toxin-antitoxin modules: classification, functions, and association with persistence. *Curr. Res Micro. Sci.* **2**, 100047 (2021).
32. Ramage, H. R., Connolly, L. E. & Cox, J. S. Comprehensive functional analysis of Mycobacterium tuberculosis toxin-antitoxin systems: implications for pathogenesis, stress responses, and evolution. *PLoS Genet* **5**, e1000767 (2009).
33. Sala, A., Bordes, P. & Genevaux, P. Multiple toxin-antitoxin systems in Mycobacterium tuberculosis. *Toxins (Basel)* **6**, 1002–1020 (2014).
34. Freire, D. M. et al. An NAD(+) Phosphorylase Toxin Triggers Mycobacterium tuberculosis Cell Death. *Mol. Cell* **73**, 1282–1291.e1288 (2019).
35. Tandon, H., Sharma, A., Sandhya, S., Srinivasan, N. & Singh, R. Mycobacterium tuberculosis Rv0366c-Rv0367c encodes a non-canonical PezAT-like toxin-antitoxin pair. *Sci. Rep.* **9**, 1163 (2019).
36. Ahidjo, B. A. et al. VapC toxins from Mycobacterium tuberculosis are ribonucleases that differentially inhibit growth and are neutralized by cognate VapB antitoxins. *PLoS One* **6**, e21738 (2011).
37. Agarwal, S. et al. System-Wide Analysis Unravels the Differential Regulation and In Vivo Essentiality of Virulence-Associated Proteins B and C Toxin-Antitoxin Systems of Mycobacterium tuberculosis. *J. Infect. Dis.* **217**, 1809–1820 (2018).
38. Tiwari, P. et al. MazF ribonucleases promote Mycobacterium tuberculosis drug tolerance and virulence in guinea pigs. *Nat. Commun.* **6**, 6059 (2015).
39. Arcus, V. L., McKenzie, J. L., Robson, J. & Cook, G. M. The PIN-domain ribonucleases and the prokaryotic VapBC toxin-antitoxin array. *Protein Eng. Des. Sel.* **24**, 33–40 (2011).
40. Wall, D. & Kaiser, D. Type IV pili and cell motility. *Mol. Microbiol* **32**, 1–10 (1999).
41. Senissar, M., Manav, M. C. & Brodersen, D. E. Structural conservation of the PIN domain active site across all domains of life. *Protein Sci.* **26**, 1474–1492 (2017).
42. Santos-Sierra, S., Pardo-Abarrio, C., Giraldo, R. & Diaz-Orejas, R. Genetic identification of two functional regions in the antitoxin of the parD killer system of plasmid R1. *FEMS Microbiol Lett.* **206**, 115–119 (2002).
43. Winther, K. S., Brodersen, D. E., Brown, A. K. & Gerdes, K. VapC20 of Mycobacterium tuberculosis cleaves the sarcin-ricin loop of 23S rRNA. *Nat. Commun.* **4**, 2796 (2013).
44. Cruz, J. W. et al. Growth-regulating Mycobacterium tuberculosis VapC-mt4 toxin is an isoacceptor-specific tRNase. *Nat. Commun.* **6**, 7480 (2015).
45. Cruz, J. W. & Woychik, N. A. tRNAs taking charge. *Pathog. Dis.* **74**, ftv117 (2016).
46. Chauhan, U., Barth, V. C. & Woychik, N. A. tRNA(fMet) Inactivating Mycobacterium tuberculosis VapBC Toxin-Antitoxin Systems as Therapeutic Targets. *Antimicrob. Agents Chemother.* **66**, e0189621 (2022).
47. Gupta, A., Venkataraman, B., Vasudevan, M. & Gopinath Bankar, K. Co-expression network analysis of toxin-antitoxin loci in Mycobacterium tuberculosis reveals key modulators of cellular stress. *Sci. Rep.* **7**, 5868 (2017).
48. Zhang, L. Y. et al. Toxin-Antitoxin Systems Alter Adaptation of Mycobacterium smegmatis to Environmental Stress. *Microbiol Spectr.* **10**, e0281522 (2022).
49. Sharma, A. et al. HigB1 Toxin in Mycobacterium tuberculosis Is Upregulated During Stress and Required to Establish Infection in Guinea Pigs. *Front Microbiol* **12**, 748890 (2021).
50. Gosain T. P., Singh M., Singh C., Thakur K. G., Singh R. Disruption of MenT2 toxin impairs the growth of Mycobacterium tuberculosis in guinea pigs. *Microbiology (Reading)* **168**, (2022).
51. Gosain, T. P. et al. Mycobacterium tuberculosis strain with deletions in menT3 and menT4 is attenuated and confers protection in mice and guinea pigs. *Nat. Commun.* **15**, 5467 (2024).
52. Zaveri, A. et al. Depletion of the DarG antitoxin in Mycobacterium tuberculosis triggers the DNA-damage response and leads to cell death. *Mol. Microbiol* **114**, 641–652 (2020).
53. Sharma, A. et al. VapC21 Toxin Contributes to Drug-Tolerance and Interacts With Non-cognate VapB32 Antitoxin in Mycobacterium tuberculosis. *Front Microbiol* **11**, 2037 (2020).
54. Singh, R., Barry, C. E. 3rd & Boshoff, H. I. The three RelE homologs of Mycobacterium tuberculosis have individual, drug-specific effects on bacterial antibiotic tolerance. *J. Bacteriol.* **192**, 1279–1291 (2010).
55. Han, J. S. et al. Characterization of a chromosomal toxin-antitoxin, Rv1102c-Rv1103c system in Mycobacterium tuberculosis. *Biochem Biophys. Res Commun.* **400**, 293–298 (2010).

56. Gupta, A. Killing activity and rescue function of genome-wide toxin-antitoxin loci of Mycobacterium tuberculosis. *FEMS Microbiol Lett.* **290**, 45–53 (2009).
57. Chattopadhyay, G. et al. Functional and Biochemical Characterization of the MazEF6 Toxin-Antitoxin System of Mycobacterium tuberculosis. *J. Bacteriol.* **204**, e0005822 (2022).
58. Betts, J. C., Lukey, P. T., Robb, L. C., McAdam, R. A. & Duncan, K. Evaluation of a nutrient starvation model of Mycobacterium tuberculosis persistence by gene and protein expression profiling. *Mol. Microbiol* **43**, 717–731 (2002).
59. Rustad, T. R., Harrell, M. I., Liao, R. & Sherman, D. R. The enduring hypoxic response of Mycobacterium tuberculosis. *PLoS One* **3**, e1502 (2008).
60. Voskuil, M. I., Bartek, I. L., Visconti, K. & Schoolnik, G. K. The response of mycobacterium tuberculosis to reactive oxygen and nitrogen species. *Front Microbiol* **2**, 105 (2011).
61. Sherman, B. T. et al. DAVID: a web server for functional enrichment analysis and functional annotation of gene lists (2021 update). *Nucleic Acids Res* **50**, W216–W221 (2022).
62. Ward, S. K., Hoye, E. A. & Talaat, A. M. The global responses of Mycobacterium tuberculosis to physiological levels of copper. *J. Bacteriol.* **190**, 2939–2946 (2008).
63. Marcus, S. A., Sidiropoulos, S. W., Steinberg, H. & Talaat, A. M. CsoR Is Essential for Maintaining Copper Homeostasis in Mycobacterium tuberculosis. *PLoS One* **11**, e0151816 (2016).
64. Festa, R. A. et al. A novel copper-responsive regulon in Mycobacterium tuberculosis. *Mol. Microbiol* **79**, 133–148 (2011).
65. Belardinelli, J. M. et al. Biosynthesis and translocation of unsulfated acyltrehaloses in Mycobacterium tuberculosis. *J. Biol. Chem.* **289**, 27952–27965 (2014).
66. Kumar, P. et al. PapA1 and PapA2 are acyltransferases essential for the biosynthesis of the Mycobacterium tuberculosis virulence factor sulfolipid-1. *Proc. Natl Acad. Sci. USA* **104**, 11221–11226 (2007).
67. Fenn, K., Wong, C. T. & Darbari, V. C. Mycobacterium tuberculosis Uses Mce Proteins to Interfere With Host Cell Signaling. *Front Mol. Biosci.* **6**, 149 (2019).
68. Lee, W., VanderVen, B. C., Fahey, R. J. & Russell, D. G. Intracellular Mycobacterium tuberculosis exploits host-derived fatty acids to limit metabolic stress. *J. Biol. Chem.* **288**, 6788–6800 (2013).
69. Kalscheuer, R., Weinrick, B., Veeraraghavan, U., Besra, G. S. & Jacobs, W. R. Jr. Trehalose-recycling ABC transporter LpqY-SugA-SugB-SugC is essential for virulence of Mycobacterium tuberculosis. *Proc. Natl Acad. Sci. USA* **107**, 21761–21766 (2010).
70. Bartek, I. L. et al. Mycobacterium tuberculosis Lsr2 is a global transcriptional regulator required for adaptation to changing oxygen levels and virulence. *mBio* **5**, e01106–e01114 (2014).
71. Cumming B. M., et al. The Physiology and Genetics of Oxidative Stress in Mycobacteria. *Microbiol Spectr* **2**, (2014).
72. Kumar, P., Amara, R. R., Challu, V. K., Chadda, V. K. & Satchidanandam, V. The Apa protein of Mycobacterium tuberculosis stimulates gamma interferon-secreting CD4+ and CD8+ T cells from purified protein derivative-positive individuals and affords protection in a guinea pig model. *Infect. Immun.* **71**, 1929–1937 (2003).
73. Garces, A. et al. EspA acts as a critical mediator of ESX1-dependent virulence in Mycobacterium tuberculosis by affecting bacterial cell wall integrity. *PLoS Pathog.* **6**, e1000957 (2010).
74. Puri, R. V., Reddy, P. V. & Tyagi, A. K. Secreted acid phosphatase (SapM) of Mycobacterium tuberculosis is indispensable for arresting phagosomal maturation and growth of the pathogen in guinea pig tissues. *PLoS One* **8**, e70514 (2013).
75. Pal, R., Bisht, M. K. & Mukhopadhyay, S. Secretory proteins of Mycobacterium tuberculosis and their roles in modulation of host immune responses: focus on therapeutic targets. *FEBS J.* **289**, 4146–4171 (2022).
76. Lou, Y., Rybniker, J., Sala, C. & Cole, S. T. EspC forms a filamentous structure in the cell envelope of Mycobacterium tuberculosis and impacts ESX-1 secretion. *Mol. Microbiol* **103**, 26–38 (2017).
77. Sanchez-Barinas, C. D. et al. Mycobacterium tuberculosis H37Rv LpqG Protein Peptides Can Inhibit Mycobacterial Entry through Specific Interactions. *Molecules* **23**, 526 (2018).
78. Qian, J., Chen, R., Wang, H. & Zhang, X. Role of the PE/PPE Family in Host-Pathogen Interactions and Prospects for Anti-Tuberculosis Vaccine and Diagnostic Tool Design. *Front Cell Infect. Microbiol* **10**, 594288 (2020).
79. Kasari, V., Mets, T., Tenson, T. & Kaldalu, N. Transcriptional cross-activation between toxin-antitoxin systems of Escherichia coli. *BMC Microbiol* **13**, 45 (2013).
80. Mishra, S. et al. Efficacy of beta-lactam/beta-lactamase inhibitor combination is linked to WhiB4-mediated changes in redox physiology of Mycobacterium tuberculosis. *Elife* **6**, e25624 (2017).
81. Gao, C. H., Yang, M. & He, Z. G. Characterization of a novel ArsR-like regulator encoded by Rv2034 in Mycobacterium tuberculosis. *PLoS One* **7**, e36255 (2012).
82. Gong, Z., Li, H., Cai, Y., Stojkoska, A. & Xie, J. Biology of MarR family transcription factors and implications for targets of antibiotics against tuberculosis. *J. Cell Physiol.* **234**, 19237–19248 (2019).
83. Mistry, J. et al. Pfam: The protein families database in 2021. *Nucleic Acids Res* **49**, D412–D419 (2021).
84. Kim, Y., Wang, X., Ma, Q., Zhang, X. S. & Wood, T. K. Toxin-antitoxin systems in Escherichia coli influence biofilm formation through YjgK (TabA) and fimbriae. *J. Bacteriol.* **191**, 1258–1267 (2009).
85. Chan, W. T., Espinosa, M. & Yeo, C. C. Keeping the Wolves at Bay: Antitoxins of Prokaryotic Type II Toxin-Antitoxin Systems. *Front Mol. Biosci.* **3**, 9 (2016).
86. De Bruyn, P., Girardin, Y. & Loris, R. Prokaryote toxin-antitoxin modules: Complex regulation of an unclear function. *Protein Sci.* **30**, 1103–1113 (2021).
87. Overgaard, M., Borch, J., Jorgensen, M. G. & Gerdes, K. Messenger RNA interferase RelE controls relBE transcription by conditional cooperativity. *Mol. Microbiol* **69**, 841–857 (2008).
88. Cataudella, I., Trusina, A., Sneppen, K., Gerdes, K. & Mitarai, N. Conditional cooperativity in toxin-antitoxin regulation prevents random toxin activation and promotes fast translational recovery. *Nucleic Acids Res* **40**, 6424–6434 (2012).
89. Meena, L. S. & Rajni Survival mechanisms of pathogenic Mycobacterium tuberculosis H37Rv. *FEBS J.* **277**, 2416–2427 (2010).
90. Chai, Q., Zhang, Y. & Liu, C. H. Mycobacterium tuberculosis: An Adaptable Pathogen Associated With Multiple Human Diseases. *Front Cell Infect. Microbiol* **8**, 158 (2018).
91. Stallings, C. L. & Glickman, M. S. Is Mycobacterium tuberculosis stressed out? A critical assessment of the genetic evidence. *Microbes Infect.* **12**, 1091–1101 (2010).
92. Wen, Y., Behiels, E. & Devreese, B. Toxin-Antitoxin systems: their role in persistence, biofilm formation, and pathogenicity. *Pathog. Dis.* **70**, 240–249 (2014).
93. Dorr, T., Vulic, M. & Lewis, K. Ciprofloxacin causes persister formation by inducing the TisB toxin in Escherichia coli. *PLoS Biol.* **8**, e1000317 (2010).
94. Keren, I., Shah, D., Spoering, A., Kaldalu, N. & Lewis, K. Specialized persister cells and the mechanism of multidrug tolerance in Escherichia coli. *J. Bacteriol.* **186**, 8172–8180 (2004).
95. Goormaghtigh F. et al. Reassessing the Role of Type II Toxin-Antitoxin Systems in Formation of Escherichia coli Type II Persister Cells. *mBio* **9**, (2018).
96. Miallau, L. et al. Comparative proteomics identifies the cell-associated lethality of M. tuberculosis RelBE-like toxin-antitoxin complexes. *Structure* **21**, 627–637 (2013).

97. Kamruzzaman M., Wu A. Y., Iredell J. R. Biological Functions of Type II Toxin-Antitoxin Systems in Bacteria. *Microorganisms* **9**, (2021).
98. Sharp, J. D. et al. Growth and translation inhibition through sequence-specific RNA binding by Mycobacterium tuberculosis VapC toxin. *J. Biol. Chem.* **287**, 12835–12847 (2012).
99. Bukowski, M., Rojowska, A. & Wladyka, B. Prokaryotic toxin-antitoxin systems-the role in bacterial physiology and application in molecular biology. *Acta Biochim Pol.* **58**, 1–9 (2011).
100. Norton, J. P. & Mulvey, M. A. Toxin-antitoxin systems are important for niche-specific colonization and stress resistance of uropathogenic Escherichia coli. *PLoS Pathog.* **8**, e1002954 (2012).
101. Schifano, J. M. et al. An RNA-seq method for defining endoribonuclease cleavage specificity identifies dual rRNA substrates for toxin MazF-mt3. *Nat. Commun.* **5**, 3538 (2014).
102. Lee, S. R. & Collins, K. Starvation-induced cleavage of the tRNA anticodon loop in Tetrahymena thermophila. *J. Biol. Chem.* **280**, 42744–42749 (2005).
103. Cintron, M. et al. Accurate target identification for Mycobacterium tuberculosis endoribonuclease toxins requires expression in their native host. *Sci. Rep.* **9**, 5949 (2019).
104. Wang, Q. et al. PE/PPE proteins mediate nutrient transport across the outer membrane of Mycobacterium tuberculosis. *Science* **367**, 1147–1151 (2020).
105. Mitra A., Speer A., Lin K., Ehrt S., Niederweis M. PPE Surface Proteins Are Required for Heme Utilization by Mycobacterium tuberculosis. *mBio* **8**, (2017).
106. Li, F. et al. Computational analysis and prediction of PE_PGRS proteins using machine learning. *Comput Struct. Biotechnol. J.* **20**, 662–674 (2022).
107. Barth, V. C. et al. Toxin-mediated ribosome stalling reprograms the Mycobacterium tuberculosis proteome. *Nat. Commun.* **10**, 3035 (2019).
108. Park, J. H., Shim, D., Kim, K. E. S., Lee, W. & Shin, S. J. Understanding Metabolic Regulation Between Host and Pathogens: New Opportunities for the Development of Improved Therapeutic Strategies Against Mycobacterium tuberculosis Infection. *Front Cell Infect. Microbiol* **11**, 635335 (2021).
109. Cabral D. J., Wurster J. I., Belenky P. Antibiotic Persistence as a Metabolic Adaptation: Stress, Metabolism, the Host, and New Directions. *Pharmaceuticals (Basel)* **11**, (2018).
110. Martinez, J. L. & Rojo, F. Metabolic regulation of antibiotic resistance. *FEMS Microbiol Rev.* **35**, 768–789 (2011).
111. Riffaud, C., Pinel-Marie, M. L. & Felden, B. Cross-Regulations between Bacterial Toxin-Antitoxin Systems: Evidence of an Interconnected Regulatory Network? *Trends Microbiol* **28**, 851–866 (2020).
112. Vilcheze, C., Weinrick, B., Leung, L. W. & Jacobs, W. R. Jr. Plasticity of Mycobacterium tuberculosis NADH dehydrogenases and their role in virulence. *Proc. Natl Acad. Sci. USA* **115**, 1599–1604 (2018).
113. Bhargavi G., et al. Role of a Putative Alkylhydroperoxidase Rv2159c in the Oxidative Stress Response and Virulence of Mycobacterium tuberculosis. *Pathogens* **11**, (2022).
114. McGillivray, A., Golden, N. A., Gautam, U. S., Mehra, S. & Kaushal, D. The Mycobacterium tuberculosis Rv2745c plays an important role in responding to redox stress. *PLoS One* **9**, e93604 (2014).
115. Ng, V. H., Cox, J. S., Sousa, A. O., MacMicking, J. D. & McKinney, J. D. Role of KatG catalase-peroxidase in mycobacterial pathogenesis: countering the phagocyte oxidative burst. *Mol. Microbiol* **52**, 1291–1302 (2004).
116. Ehrt, S. et al. Controlling gene expression in mycobacteria with anhydrotetracycline and Tet repressor. *Nucleic Acids Res* **33**, e21 (2005).
117. Bardarov, S. et al. Specialized transduction: an efficient method for generating marked and unmarked targeted gene disruptions in Mycobacterium tuberculosis, M. bovis BCG and M. smegmatis. *Microbiol. (Read.)* **148**, 3007–3017 (2002).
118. Li, H. et al. The Sequence Alignment/Map format and SAMtools. *Bioinformatics* **25**, 2078–2079 (2009).
119. Arun, Sharma, et al. Transcriptome analysis of VapC13 and VapC26 overexpression in Mycobacterium tuberculosis. In: *NCBI* https://www.ncbi.nlm.nih.gov/bioproject/PRJNA996620 (2024).
120. Priyanka, A., Solanki, V., Parkesh, R. & Thakur, K. G. Crystal structure of the N-terminal domain of human SIRT7 reveals a three-helical domain architecture. *Proteins* **84**, 1558–1563 (2016).

Acknowledgements

This work was supported by the DBT/Wellcome Trust India Alliance Fellowship (IA/S/19/2/504646) awarded to RS. RS is a recipient of the National Bioscience Award from the Department of Biotechnology and Ramalingaswami fellowship. RV acknowledges support from the DST JC Bose Fellowship and infrastructural support from DST-FIST. AS is a recipient of senior research fellowship from the Indian Council for Medical Research (Fellowship/TB/43/2020-ECD-1). NS acknowledges the research fellowship by the Department of Biotechnology. MB is thankful to the Council of Scientific and Industrial Research for her fellowship. Professor Nagasuma Chandra from the Department of Biochemistry, Indian Institute of Science, is acknowledged for kindly sharing the network analysis pipeline utilised for this study. The authors sincerely thank Ms. Manisha Singh for the generation of Δ*vapBC26* strain of *M. tuberculosis*. The authors are thankful to staff members of the biosafety level 3 facility and experimental animal facility at the Translational Health Science and Technology Institute for their help. The authors are also thankful to the National Liver Disease Biobank staff members at the Institute of Liver and Biliary Diseases for histopathology analysis. The authors acknowledge Mr. Saqib Kidwai for help with aerosol infections. The authors sincerely acknowledge the help of Mr. Ashish Kumar, Mr. Rajesh and Mr Sher Singh in performing experiments. The funders had no role in the study design, results, analysis, or manuscript preparation.

Author contributions

RS conceived the idea and designed the work plan. AS, NS, PT and PC performed the microbiology and molecular biology experiments. AS and MB performed the RNA sequencing data curation and analysis. AS, NS and PT performed the animal experiments. RS and RV supervised the experiments. RS and AS analysed and interpreted the data. RS and AS wrote the manuscript with inputs from other authors.

Competing interests

The authors declare that this study was conducted in the absence of any commercial or financial relationships that could be considered a potential conflict of interest.

Additional information

Supplementary information The online version contains supplementary material available at https://doi.org/10.1038/s42003-024-06998-6.

Correspondence and requests for materials should be addressed to Ramandeep Singh.

Peer review information *Communications Biology* thanks Xibing Xu and the other, anonymous, reviewer(s) for their contribution to the peer review of this work. Primary Handling Editors: Si Ming Man and Tobias Goris. A peer review file is available.